STUDIES ON SELECTIVE GELATION PRINTING AND MICROWAVE SINTERING OF ALUMINA AND ZIRCONIA SAMPLES

BY

OZAN UGURLU

A THESIS
SUBMITTED TO THE FACULTY OF

ALFRED UNIVERSITY

IN PARTIAL FULFILLMENT OF THE REQUIREMENTS
FOR THE DEGREE OF

MASTER OF SCIENCE

IN

CERAMIC ENGINEERING

ALFRED, NEW YORK

FEBRUARY, 2003

STUDIES ON SELECTIVE GELATION PRINTING AND MICROWAVE SINTERING OF ALUMINA AND ZIRCONIA SAMPLES

BY

OZAN UGURLU

B.S. MIDDLE EAST TECHNICAL UNIVERSITY (2001)

SIGNATURE OF AUTHOR (Signature on file)

APPROVED BY (Signature on file)
HERBERT GIESCHE, ADVISOR

(Signature on file)
DAVID A. EARL, ADVISORY COMMITTEE

(Signature on file)
WALTER A. SCHULZE, ADVISORY COMMITTEE

(Signature on file)
ALEXIS CLARE, CHAIR, ORAL THESIS DEFENSE

ACCEPTED BY (Signature on file)
RONALD S. GORDON, DEAN,
SCHOOL OF CERAMIC ENGINEERING
AND MATERIALS SCIENCE

ACKNOWLEDGMENTS

First I would like to thank my advisor Dr. Herbert Giesche for his support, encouragement and giving me the chance to work on my Master of Science thesis with him in the New York State College of Ceramics at Alfred University. He never got tired of helping me, even it was mid-night. I also thank him for being such a great friend as well as an advisor, during these one and a half years. Also I would like to thank Joseph J. Stanco from Metrix Composites, Inc. (Utica, NY) for his financial support, guidance and patience. I also thank him for allowing me to conduct some of my experiments in Metrix Composites, Inc. and for all of his assistance during that time.

NYSERDA, Metrix Composites, Ceralink and Center for Advanced Ceramic Technologies (CACT) are acknowledged for their support to make this project possible.

I would like to thank Dr. David Earl and Dr. Walter Schulze for their help with my committee. Their insight and views help me to complete my thesis.

Next I would like to thank, Ward Votova for teaching me how to use the SEM, Hamilton Black for his extensive help in the laboratory, Gary Del Regno for correcting my thesis and assisting me in setting up the microwave tests, and Morgana Fall for taking her time to help me on CPI Autowave. I also would like to thank to my family for all of their support throughout my life and to all my friends both in USA and Turkey.

Last but certainly not least, I would like to thank to a very special friend Seda Salebci. Her invaluable and continuous support meant a lot to me. Thank you for being there for me whenever I needed an angel.

TABLE OF CONTENTS

I INTRODUCTION 1

II LITERATURE SURVEY 2

A. What is Rapid Prototyping? 2

1. Examples of Rapid Prototyping Processes for Ceramic Products 2
2. Selective Gelation Printing 3

B. Slurry Dispersion 6

1. Electrostatic Dispersion 6
2. Steric Dispersion 6
3. Electrosteric Dispersion 7
4. Zeta Potential 8

C. Microwave 11

1. Microwave Sintering 11
2. Interaction of Materials with Microwaves 11

III EXPERIMENTAL PROCEDURE 14

A. Slurry Preparation and Characterization 14

B. Mapping and Optimization of MW sintering 16

C. Microwave and Conventional Sintering of SGP Printed Samples 21

D. Density Measurements (Archimedes') 22

E. Sample Characterization 22

IV RESULTS AND DISCUSSIONS 24

A. Slurry Preparation and Characterization 24

1. Shear Thinning Effect 24
2. Effect of Darvan on Viscosity 25
3. Effect of Solid Loading on Viscosity 26
4. Zeta Potential Measurements 27

B. Mapping and Optimization of MW sintering 29

1. Mapping of the CPI Autowave Microwave Furnace 29
2. Temperature and Time Effects on Sintered Density During MW Sintering 32
3. Heat-up Rate Comparison (MW vs Conventional) 37
4. Optimization of Thermal Etching and Grain Size Measurement 41
5. Microstructure Characterization 48
6. Effect of Number of "Boxes" On Temperature 63
7. Energy Consumption Comparison (MW vs Conventional heating) 65

C. Microwave and Conventional Sintering of SGP Printed Samples 66

V CONCLUSION 68
VI FUTURE WORK 70
REFERENCES 71
APPENDIX 74

LIST OF TABLES

Table III-I CPI Autowave and Raytek Pyrometer Specifications 17

Table III-II Power-Time Profile..... 19

Table III-III Temperature & Dwell Time Matrix of (a) Zirconia and (b)Alumina. 20

Table III-IV Compositions of Slurries Used in SGP printing. 21

Table IV-I Densities of the Zirconia Samples 29

Table IV-II Characterization Values of Microwave Sintered Zirconia Samples 33

Table IV-III Characterization Values of Microwave Sintered Alumina Samples..... 34

Table IV-IV Heat-up Rates of Microwave and Conventional Sintering. 37

Table IV-V Theoretical Densities of the Printed Samples of Different Slurries..... 66

LIST OF FIGURES

Figure II-1 Schematic drawing of Selective Gelation Process 4

Figure II-2 (a) 1-4-Linked β-D-Mannopyranosyluronic acid unit
(b) 1-4-Linked α-L-Gulopyranosyluronic acid unit. 4

Figure II-3 G-Block polymer. 5

Figure II-4 Schematic figure showing the gelation of G-Block alginate
by calcium ion addition 5

Figure II-5 Schematic drawing of dispersed alumina particles 7

Figure II-6 Ammonium Polyacrylate 7

Figure II-7 Normalized mobility as a function of particle size and frequency 9

Figure II-8 Schematic drawing of the Acustosizer cell. 10

Figure III-1 Slurry preparation flow diagram 15

Figure III-2 (a) Insulation Box, Thermceptors and the sample
(b) Schematic drawing of the insulation box 18

Figure III-3 Schematic drawing of CPI Autowave microwave furnace. 19

Figure IV-1 Viscosity change as a function of shear rate. 24

Figure IV-2 Viscosity change as a function of dispersant content. 25

Figure IV-3 Viscosity change of alumina and zirconia as a function
of solid content. 26

Figure IV-4 Zeta-potential change as a function of pH
(a) alumina
(b) zirconia 28

Figure IV-5 Mapping of CPI Autowave microwave furnace cavity 31

Figure IV-6 Pyrometer setup. 32

Figure IV-7 Hardness values of the microwave sintered zirconia samples vs. dwell time. 35

Figure IV-8 Hardness and porosity of the microwave sintered zirconia samples at 1460°C. 35

Figure IV-9 Hardness and porosity of the microwave sintered alumina samples at 1500°C. 36

Figure IV-10 Heat-up rates of conventional and MW sintering. 37

Figure IV-11 Heating curves of zirconia and alumina samples. 39

Figure IV-12 (a) Alumina sample grinded with SiC paper, (b) Alumina sample grinded with diamond wheel. 41

Figure IV-13 Thermal etching of zirconia at 1450°C. 43

Figure IV-14 Thermal etching of zirconia at 1350°C. 44

Figure IV-15 Thermal etching of zirconia at 1250°C. 45

Figure IV-16 SEM micrograph of sample Z42, thermal etched at 1000°C. 46

Figure IV-17 (a) Filtered SEM micrograph, (b) Outlined SEM micrograph, (c) Scanned image 47

Figure IV-18 (a) & (b) Micrographs of microwave sintered zirconia at 4 different dwell times and at 1440°C. 48

Figure IV-18 (c) & (d) Micrographs of microwave sintered zirconia at 4 different dwell times and at 1440°C. 49

Figure IV-19 (a) & (b) Micrographs of microwave sintered zirconia at 4 different dwell times and at 1460°C. 50

Figure IV-19 (c) & (d) Micrographs of microwave sintered zirconia at 4 different dwell times and at 1460°C. 51

Figure IV-20 (a) & (b) Micrographs of microwave sintered zirconia at 4 different dwell times and at 1480°C. 52

Figure IV-20 (c) & (d) Micrographs of microwave sintered zirconia at 4 different dwell times and at 1480°C. 53

Figure IV-21 Grain size distribution of microwave sintered zirconia samples with different dwell times at 1460°C. 54

Figure IV-22 Grain size distribution of microwave sintered zirconia samples at different temperatures with 10 min. dwell time. 54

Figure IV-23 Average grain sizes of the microwave sintered zirconia samples at different temperatures and dwell times. 55

Figure IV-24 (a) & (b) Micrographs of microwave sintered alumina at different temperatures and dwell times..... 586

Figure IV-24 (c) & (d) Micrographs of microwave sintered alumina at different temperatures and dwell times..... 57

Figure IV-24 (e) Micrographs of microwave sintered alumina at different temperatures and dwell times..... 58

Figure IV-25 Grain size distribution of microwave sintered alumina samples with different dwell times at 1500°C. 58

Figure IV-26 Grain size distribution of microwave sintered alumina samples at different temperatures with 15 min. dwell time. 59

Figure IV-27 Micrographs of sintered alumina
(a) conventional
(b) microwave. 60

Figure IV-28 (a) Micrograph of microwave sintered alumina sample 621

Figure IV-28 (b) Micrograph of microwave sintered zirconia sample 62

Figure IV-29 Grain size distribution of microwave sintered alumina and zirconia. 62

Figure IV-30 Temperature reading for single and 2 boxes at a time. 64

Figure IV-31 Temperature and energy graph for MW sintering of alumina. 65

Figure IV-32 Temperature and energy graph for conventional sintering of alumina. 65

ABSTRACT

Selective Gelation Printing (SGP) is a new Rapid Prototyping (RP) technique for producing complex shaped ceramic parts. The method is based on gelation of ceramic powder slurries containing alginate binder with specific multivalent cations to build high green density ceramic bodies. When this technique is combined with microwave sintering, it becomes a very fast and energy efficient ceramic processing method. In the present study, the effect of different parameters on viscosities of Selective Gelation Printing slurries were studied, as well as sintering temperature and time effects on final density of microwave sintered samples. These samples were characterized with respect to hardness, density and grain size differences. In addition, energy consumption and temperature ramp rates of microwave and conventional heating were compared. Similar high densities were achieved with microwave sintering and conventional sintering. Microwave sintering cycles were much shorter in comparison to conventional sintering process. Also, microwave sintering proved to be more energy efficient compared to conventional sintering based on manufacturing of individual samples.

I INTRODUCTION

The main goal of this study was to develop a fast and energy-saving ceramic processing technique. This study combines Selective Gelation Printing, a layered manufacturing technique with microwave sintering to decrease the total production time of a ceramic part from powder to sintered form. This technique can be useful especially in applications which require a custom designed product, as for example, in the production of ceramic medical implants like knee or hip implants.

Selective Gelation Printing (SGP) is one of the few ceramic layered manufacturing techniques. Selective Gelation Printing is superior to other ceramic rapid prototyping techniques, because of its high solid and low binder containing slurries. This gives high green density products which increases the final sintered density.

The present study focuses on optimization of alumina and zirconia gel-based slurries having low viscosity and high solid contents for Selective Gelation Printing. Another focus of the study was to map the CPI Autowave microwave furnace to identify hot and cold spots and locate the optimum area and time-temperature profiles for microwave sintering. Microwave sintering has many advantages, when compared to conventional sintering. Volumetric heating, faster sintering times, and lower energy consumption are among these advantages.

II LITERATURE SURVEY

A. What is Rapid Prototyping?

Rapid prototyping (RP), also called solid free form fabrication, automates the fabrication of a prototype part from a three-dimensional (3-D) CAD drawing. A prototype model shows preliminary information about a product. Production times may take weeks or even months for conventional prototyping; but it takes only a few days for a rapid prototyping process.[1] Rapid prototyping can be quicker and more cost-effective than conventional methods. Companies like Metrix Composites are extending RP towards "layered manufacturing" of ceramic parts at low costs.

Prototyping processes can be divided into three categories: Compressive, additive and subtractive. Compressive processes force a semi-solid or liquid material into a predetermined fixed shape, then hardens or solidifies the product. Additive processes join particles or layers to get the desired shape or product. Subtractive processes produce the desired object by carving it out from a block of material. Most rapid prototyping systems use additive processing while conventional prototyping uses subtractive processing.

Rapid prototyping processes can be classified according to the materials they are using: Photopolymers, thermoplastics, or adhesives. RP techniques which produce ceramic parts are still under development and they are either extensions of polymer methods, where matrix resins are loaded with powder, or processes that use layers of ceramic powders.

1. Examples of Rapid Prototyping Processes for Ceramic Products

Stereolithography of ceramics uses thin layers of photocurable resins, which contain ceramic powders. Selected areas on the layers are cured with an ultraviolet laser, and ceramic products are produced by repeating layering and curing processes.[2]

Robocasting, fused deposition and extrusion techniques use injection or extrusion of temperature-sensitive suspensions of ceramic powders to build ceramic parts.[3]

In Selective-Laser-Sintering (SLS), a ceramic part is generated by local sintering of powder layers with a computer controlled laser. Final products are produced by repeating the local sintering and layering processes.[4, 5]

Three-Dimensional Printing (3DP) again uses powder layers but this time powders are 'solidified' selectively by depositing a binder through an ink-jet printer head.[6-8]

Tape-lamination method such as CAM-LAM uses ceramic green tapes with a high solid loading. A controlled laser cuts the green tape into a desired shape. After cutting each layer, a new layer is laminated to the previous layer. This process continues repeatedly to achieve the final shape. After binder burn-out ceramic parts are sintered to high density.[9, 10]

Using tapes or suspensions may, in most cases, be better in terms of packing density, then using powder beds. Fabricating high-density parts from powder beds can be more difficult because of their low packing density. However, MIT has developed slurry based printing to achieve higher packing densities.

2. Selective Gelation Printing

Selective Gelation Printing (SGP) is a new rapid prototyping technique which is able to produce ceramic parts. SGP uses alginate gelation as the key process in this technique. In Selective Gelation Printing slurry which contains alginate and high ceramic powder contents (~50 vol %) is layered over a build table with the help of a doctor blade. Calcium ions are inkjet printed locally on to that layer of slurry and the alginate turns into a gel, thus forming a 3D network that immediately entraps the ceramic powders at those local points. Those steps are repeated layer by layer until the desired part is finished in its gelled form (Fig. II-1). At the end, the gelled part is removed from the slurry, washed, dried and sintered into the final shape. Washing of the gelled part in deionized water lowers the cation concentration to parts-per-million (ppm) levels in the final sintered ceramic body.[11]

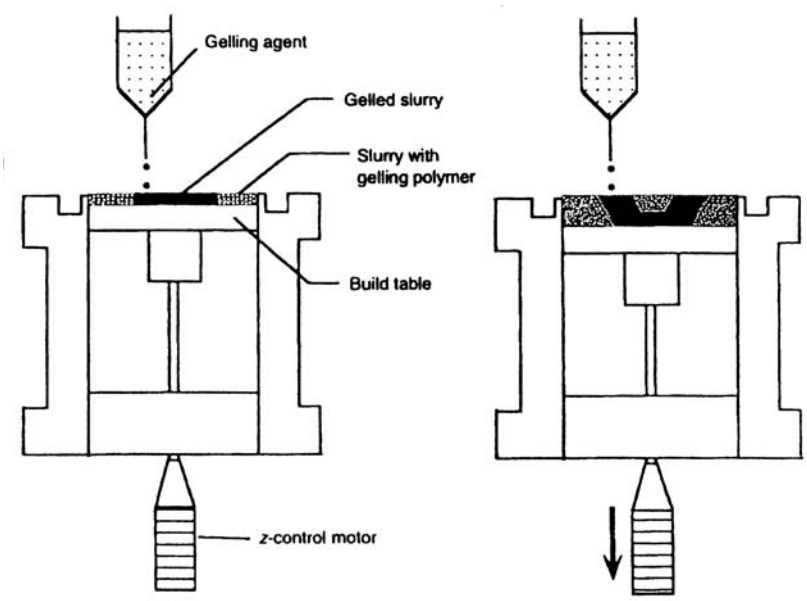

Figure II-1. Schematic drawing of Selective Gelation Process.[12]

Alginic acid is an inexpensive polysaccharide, and it has been used in the food industry for a long time. Alginates have the ability to form strong gels even at low concentrations, as low as 0.4 wt% alginate in water would be enough for forming a sufficiently strong gel structure. This ability makes them very useful for SGP. Alginate polymer consist of two monomeric units, β-D-mannuronopyranosyl and α-L-guluronopyranosyl units. (Fig. II-2)

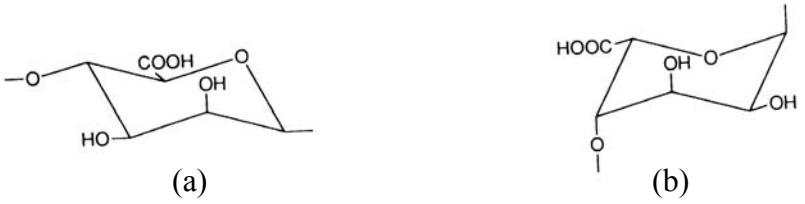

(a) (b)

Figure II-2. (a) 1-4-Linked β-D-Mannopyranosyluronic acid unit.[11]
(b) 1-4-Linked α-L-Gulopyranosyluronic acid unit.[11]

Those monomers occur in the alginate polymer as blocks, and blocks made from β-D-mannuronopyranosyl are called M-Blocks, while blocks made from α-L-guluronopyranosyl are called G-Blocks. (Fig. II-3)

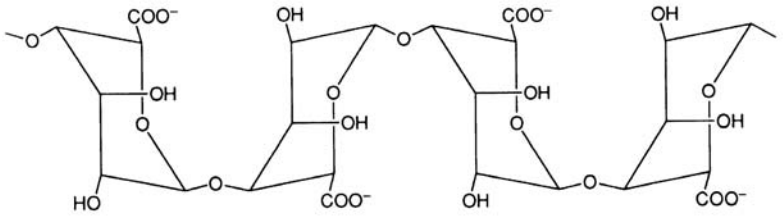

Figure II-3. G-Block polymer.[11]

An alginate polymer contains both M-Block and G-Block, but it is the G-Block which under goes gelation in the presence of calcium ions or other multivalent ions. Addition of calcium ions link the G-Blocks of different alginate polymer strands. By the help of its buckled shape, 2 G-Block chains bind together. Alignment forms a diamond-shaped hole with a hydrophilic cavity which binds the calcium ions using various oxygen atoms. As a result calcium ions bond the chains to each other, while themselves sitting in the cavity between them.[11] (Fig. II-4)

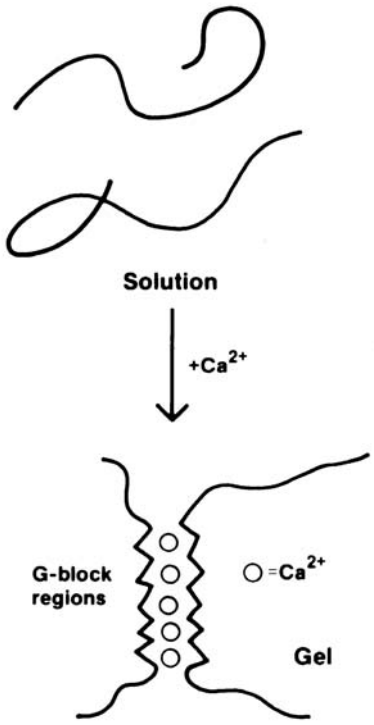

Figure II-4. Schematic figure showing the gelation of G-Block alginate by calcium ion addition.[11]

Alginates are water soluble and this makes them usable in many of the traditional ceramic applications. Alginates are used in traditional ceramics as binders, lubricants, plasticizers and suspending aids.[12]

B. Slurry Dispersion

Slurry particles tend to flocculate under the influence of Van der Waals forces. To counter-balance the Van der Waals forces a repulsive force between particles is required and this can be achieved through the use of dispersion aids. Generally there are three types of dispersion, electrostatic, steric and electrosteric dispersion.

1. Electrostatic Dispersion

When dispersion is achieved by electrostatic charge repulsions between equally charged particles, it is called electrostatic stabilization or dispersion. The ways of acquiring a surface charge on particles are: preferential adsorption of ions, dissociation of surface groups, isomorphic substitution, adsorption of polyelectrolytes and accumulation of electrolytes.[13] In the process of preferential adsorption of ions from the solution, the surface of oxide particles positively charged at low pH and negatively charged at high pH. The potential (or charge) is measured at a short distance from the particle surface (surface of shear). This potential is called ζ (zeta) potential. The isoelectric point (IEP) is the pH where the charge at the surface of shear is zero, in other words where the zeta potential is zero. Surface of shear is the surface in which the relative motion of a moving particle sets in between the immobilized layer and the mobile liquid. It is fairly close to stern layer.

2. Steric Dispersion

In steric dispersion, repulsion is produced by polymer molecules which are adsorbed or chemically attached onto the particle surfaces. Polymer chains having two specific ends, one soluble and one insoluble, are required. The insoluble end connects (chemically or physically) to the particle, and the soluble end blends with the liquid. The soluble part is like a flexible chain and the overlapping of those chains creates repulsion between particles. (Fig. II-5)

Figure II-5. Schematic drawing of dispersed alumina particles.[14]

Temperature has a significant effect on steric dispersions when compared with electrostatic dispersion. At a certain temperature which is called Θ (theta) temperature, slurry behaves like an ideal solution. At temperatures higher than Θ, coils repel each other, so the stability of the system increases. But at temperatures lower than Θ, coils attract each other and lead to a flocculation.[15]

3. Electrosteric Dispersion

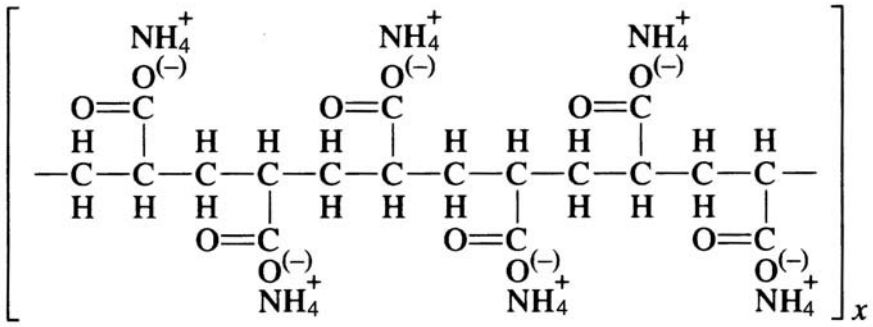

Figure II-6. Ammonium Polyacrylate.

Ammonium polyacrylate (Darvan 821A) uses both electrostatic and steric dispersion methods to disperse the particles, this is called electrosteric dispersion. In the structure of ammonium polyacrylate (Fig. II-6) hydrocarbon chain serves as a backbone lying all along the entire molecule. The molecule has branched sp^2 active groups on alternating carbon atoms $–COO^{(-)}(NH_4^+)$. For the electrostatic effect those functional

groups dissociate in water to R-COO$^-$ and the solution becomes basic so pH increases. And for the steric effect, insoluble part of the molecule anchors to the particle while wagging the tail. As described above overlapping of those tails creates repulsion between particles.

Stability of polyorganic acid structure of the polyacrylates is an important advantage over other type of dispersants like inorganic acid salts, bipolar and polypolar dispersants etc...[16]

4. Zeta Potential

a. Background Information on Calculations[17]

Zeta potential is an important guide to the stability of slurries. It shows the potential associated with the double layer. Zeta potentials of the slurries were measured by using Matec AcoustoSizer. It uses the electrokinetic sonic amplitude (ESA) effect to measure the particle size and zeta (ζ) potential. In the case of ESA, an A.C. electric field is applied across the slurry and back-and-forth electrophoretic motion of the charged particles produces a sound wave which has an amplitude proportional to the particle velocity, and this amplitude gives the dynamic mobility (μ_D) of the particles. (Dynamic mobility is the velocity of particles per unit applied field).

$$ESA = c\Delta\rho\phi f_g \mu_D \tag{1}$$

Equation 1 shows the relation between ESA and μ_D, where c is the speed of sound in the medium, $\Delta\rho$ is the density contrast between the particles and the medium, ϕ is the particle volume fraction and f_g is a geometric and acoustic coupling factor that depends on the measurement system. Particle properties are determined from the dynamic mobility factor and the relationship between μ_D and particle properties are shown in Equation 2.

$$\mu_D = \frac{2\varepsilon\xi}{3\eta} G(\alpha)(1+f) \tag{2}$$

Where, ε is the dielectric permittivity of the medium, η is the viscosity, ξ is the zeta potential, G(α) measures the effect of inertia, and f is a complex form factor for the electric field but it may be set to 0.5 for aqueous ceramic suspensions. Then Equation 2 can be simplified to Equation 3.

$$\mu_D = \mu_E G(\alpha) \tag{3}$$

Where, $\alpha=(\omega a^2/\nu)$ ω is the angular frequency of the applied field, a is the particle radius, ν is the kinematic viscosity. And μ_E is the electrophoretic mobility measured in a static electric field. It is defined by Smoluchowski formula (Equation 4). (V: velocity of the particles, E: instantaneous electric field)

$$V = \frac{\varepsilon \xi E}{\eta} \Rightarrow \frac{V}{E} = \mu_E = \frac{\varepsilon \xi}{\eta} \tag{4}$$

Figure II-7 shows the effect of particle size and frequency on the inertial response. The inertial response plotted as the normalized mobility (μ_D/μ_E) using density values for α-alumina particles in water.

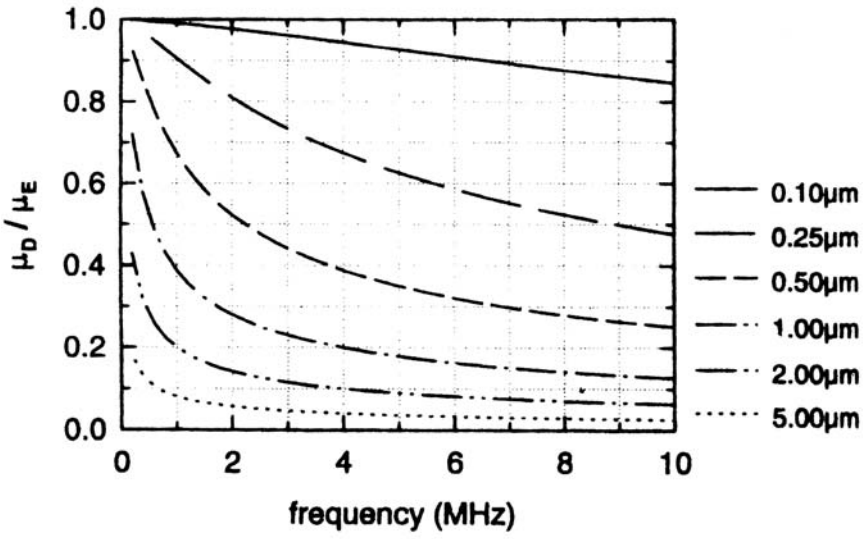

Figure II-7. Normalized mobility as a function of particle size and frequency.[17]

If the measurements made over a range of frequencies and since both the magnitude and phase of $G(\alpha)$ depend on frequency, ξ and particle size can be calculated by using the measurements of the dynamic mobility spectrum.[18]

b. Working Principles

Acoustosizer is a second generation instrument in its field. It has the capacity to measure both particle size and zeta potential simultaneously. While, the first generation instruments require particle size information in order to calculate the zeta potential.

Acoustosizer measures the ESA effect over a range of frequencies and builds a dynamic mobility spectrum, similar to Fig. II-7, which contains necessary information to calculate ξ and particle size.

Figure II-8 shows a schematic diagram of the Acoustosizer cell. Slurry stays in the container between two electrodes. Voltage pulses, from a gated amplifier, are applied through electrodes and as a result of this electrical field, particles inside the slurry move towards the electrodes and this generates sound waves. Those sound waves are recorded in the right transducer and passed into the signal processing electronics, where the amplitude and phase of the sinusoidal component of the pulses are measured.

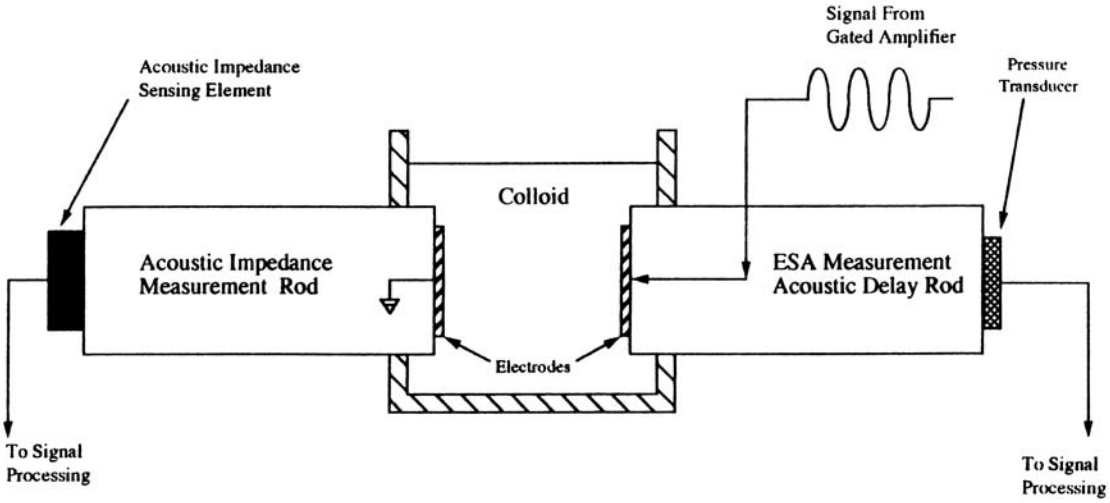

Figure II-8. Schematic drawing of the Acoustosizer cell.[18]

The ESA signal depends on the particle motion as well as the acoustic impedance of the slurry. Acoustic impedance of the slurry should be known to calculate the motion from the ESA signal. Acoustosizer measures the acoustic impedance of the slurry immediately after each measurement of ESA. This is done by using the sensors on the left hand rod, using a reflection technique, in which an acoustic pulse generated by the left sensing element travels through the rod and is partially reflected at the slurry boundary. All the data is collected on a computer after signal processing, and analyzed.

C. Microwave

1. Microwave Sintering

Microwave sintering differs from conventional sintering methods. In conventional sintering, heat is generated by external heating elements and heats up the outer surface of the sample. This heat is then transferred into the sample by thermal conduction. Since conduction is a slow process, heat-ups need to be slow enough to have minimal gradient problems, especially when sintering larger samples. However in microwave heating, heat is generated inside the sample and as a result of this internal and volumetric heating, no gradients in temperature occur within the sample. Microwave sintering is much faster and more energy efficient then conventional sintering.[19,20] Since the energy can be directed directly towards the sample and heat-up of the whole furnace can be minimized.

In addition to sintering materials, microwaves are also used for other processes like, grinding of minerals, synthesis of oxide-powders, drying[21] and also in joining of ceramic materials.[22]

2. Interaction of Materials with Microwaves[23,24]

Microwave heating uses electromagnetic waves which has a frequency range of 0.3 – 300 GHz (Wavelengths 1m – 1mm.). The most commonly used microwave frequency is 2.45 GHz. That is the primary frequency of virtually all commercial microwave ovens. Samples being sintered must have specific dielectric characteristics in order to couple with microwaves and thereby increase in temperature.

Coupling with microwaves depends on a given material complex permittivity ε^* (F/m). This is composed of two parts (Equation 5) ε' real part (dielectric constant) and ε'' imaginary part (dielectric loss factor).

$$\varepsilon^* = \varepsilon' - j\varepsilon'' = \varepsilon_0(\varepsilon_r' - j\varepsilon_{eff}'') \quad (5)$$

Where, $j=(-1)^{1/2}$, ε_0 is the permittivity of free space ($\varepsilon_0=8.86\text{x}10^{-12}$ F/m), ε_r' is the relative dielectric constant and ε_{eff}'' is the effective dielectric loss factor.

When microwaves are applied to a sample they penetrate and propagate through the sample (if the sample is an absorber material). These microwaves cause internal electric fields inside the sample. The direction of electric fields change at a rate corresponding to the frequency of the microwaves, causing movement and rotation of dipoles. But resistance of dipoles to movement and rotation causes losses and decreases the electric field. As a result of these losses the material heats up. All of the loss mechanisms are combined into the loss parameter ε_{eff}''. However loss tangent (tan δ) is used commonly in the literature (Equation 6).

$$\tan\delta = \frac{\varepsilon_{eff}''}{\varepsilon_r'} = \frac{\sigma}{2\pi f \varepsilon_0 \varepsilon_r'} \tag{6}$$

Where, σ is the total effective conductivity (S/m) generated by conduction and displacement currents. f is the frequency of the microwaves (GHz).

If we look at the power formula P (W/m^3) (Equation 7)

$$P = \sigma |E|^2 = 2\pi f \varepsilon_0 \varepsilon_r' \tan\delta |E|^2 \tag{7}$$

Where, E is the internal electric field (V/m). We can see that power absorbed by the sample varies linearly with the frequency, relative dielectric constant and tan δ. Relative dielectric constant and tan δ are both material properties. Power also varies linearly with the square of E, and E depends on the size and shape of the material.

Relative dielectric constant and tan δ are the most widely used parameters to determine the behavior of the dielectric materials under microwaves. Those parameters change as function of temperature. Some dielectrics can be transparent to microwaves at room temperature because of their low relative dielectric constant and loss tangent. But at higher temperatures than room temperature they may be high enough to increase the energy loss inside the material. This increase in ε_r' and tan δ is due to an increase in the polarizability which is caused by volumetric expansion.[25] Volumetric expansion certainly depends on the coefficient of thermal expansion. Materials which have low ε_r' and tan δ may be heated up by using a hybrid system.[19,20] Hybrid sintering uses SiC susceptors, which absorbs microwaves at room temperatures, those susceptors heat up initially within an insulation box and increase the temperature of the sample through radiant heat

transfer. Once the samples reach a critical temperature, ε_r' and tan δ will reach high enough value to allow sample to couple in microwave and sustain self-heating.

III EXPERIMENTAL PROCEDURE

This study is divided into three groups:

1. Slurry preparation and characterization
2. Mapping and optimization of microwave sintering using pressed pellets
3. Microwave and conventional sintering of SGP printed samples.

The powders and chemicals used in this study were as follows: Alumina powder (with 0.05% MgO)[*], Zirconia TOSOH-3YS Powder (94.8 wt% Zirconia, 5.2 wt% Yttria)[†], Ammonium Alginate[‡] and Darvan 821A [§].

A. Slurry Preparation and Characterization

To achieve full and homogeneous mixing of alginate solution, 2 wt% alginate solution was prepared in the overhead stirrer 24 hours before adding it to final slurry. As can be seen on Fig. III-1, slurry contents added and mixed in steps. Because of the very high solid contents, adding all the powder at the same time would turn the slurry into a solid. So, powders were added step by step and after each powder addition step they were mixed using a wrist action shaker for 10 min. After adding all contents and ball milling media (~0.25" ∅), the slurry was ball milled for at least 20 hrs. Prior to printing or testing, previously prepared alginate solution was added to the slurry and mixed with an overhead stirrer for 1 hr. All of the slurries in this study were prepared based on this method (Fig. III-1).

---

[*] RC-HP DBM, Baikowski Malakoff Industries, Inc. Malakoff, TX, USA

[†] TOSOH, Tokyo, Japan

[‡] Collatex A/RN, ISP Alginates, Inc., Wayne, NJ, USA

[§] R.T. Vanderbilt company, Inc., Norwalk, CT, USA

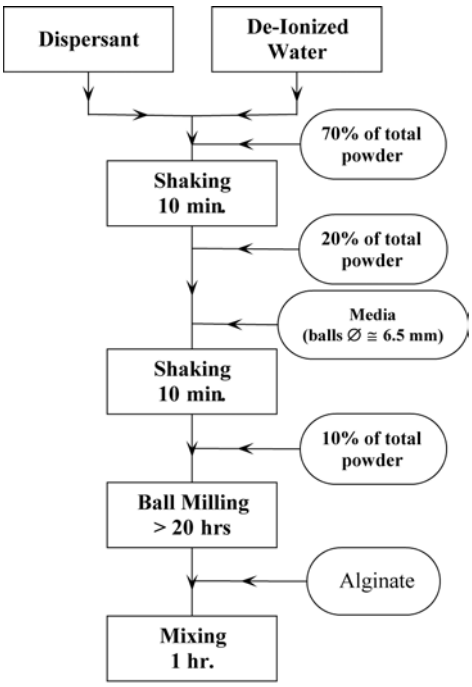

Figure III-1. Slurry preparation flow diagram.

Shear thinning behaviour of the alumina slurry was observed in a 55 vol% solid containing slurry. Viscosities were measured as a function of shear stress using a Haake* viscometer with its concentric cylinder apparatus. Different Darvan concentrations (0.55, 0.65, 0.70, 0.75 wt% based on powder) were used in this study. The effect of Darvan concentrations was further studied in next experiment.

Viscosity measurements, to see the effect of Darvan concentration, were performed on 52 vol% solid containing alumina slurry. An initial slurry was prepared containing 0.55 wt% Darvan. After ball milling for 24 hours the pH was measured using the Metrohm† pH meter and viscosity was measured using the Brookfield‡ Digital Viscometer with a T-shaped spindle. Viscosity measurements were made using 100 ml of slurry. Each 100 ml slurry sample was placed into a 300 ml beaker. The measurements were taken at 0.5" below the surface of each slurry sample and recorded after 5 minutes of equilibration time. Viscosities were recorded at four different rotation speeds (10, 20,

* Model RV-3 Karlsruhe, Germany

† Model 691, Herisau, Switzerland

‡ Model RVTDV-II, spindle #92 Middleboro, MA, USA

50 and 100 rpm) and the procedure was repeated four times, for each slurry, to obtain standard deviation. After every measurement process, the amount of Darvan was increased and the entire slurry was poured back into a ball milling jar. The new slurry was again ball milled for 12 hours and measured.

The effect of solid content on viscosity for both powder systems (alumina and zirconia) was studied, by first preparing a slurry system with the highest possible solids content. This system was then diluted by adding water. No further adjustments of the Darvan concentration were needed by using this approach. These high solids content slurries of alumina and zirconia were chosen at 60% solids volume and 51% solids volume, respectively. The Darvan content was 0.8% by weight upon the powder content of either system. The viscosity was measured as previously described. The amount of the total slurry was approximately 250ml for both of the slurry systems.

Zeta-potentials for both of the alumina and zirconia slurries were measured with the Matec Acoustosizer*. For this measurement 400 ml. slurry with 10% by volume of solids and 0.8% by weight of Darvan was used. A change in pH was observed as part of a titration series and done through high pH to low pH by using NH_3 (1M) and HCl (1M) as base and acid sources, respectively. The assumed dielectric constant of the solid particle was 12.5.

B. Mapping and Optimization of MW sintering

Tosoh TZ3YS zirconia powders were used for mapping of the CPI Autowave (see Table III-I for specifications) microwave furnace. Five gram pellets were pressed in a 1″ diameter floating die at 8000lb ≅ 6280 psi ≅ 43.3 MPa, and subsequently iso-pressed at 60000 psi ≅ 400MPa.

Individual pellets were placed inside a 3” I.D. x 4” O.D. Zircar† Al-30 cylinder. Zircar Eco-25B was used as fitted top and bottom covers. Inside the box, 2 SiC susceptors‡ (40 g. each) were used as the heating elements (Fig. III-2). The box had a

* Northborough, MA, USA

† Florida, NY, USA

‡ Research Microwave Systems, Inc

0,4” diameter hole to allow temperature monitoring with a Raytek* pyrometer. (see Table III-I for specifications).

Table III-I CPI Autowave and Raytek Pyrometer Specifications

CPI Autowave		*Raytek MA2S-C-SF pyrometer*	
Maximum Temp.	1800 °C	Temperature Range	350 – 2000 °C
Working Size	32″ x 22″ x 18″ 810 x 560 x 460mm	Focusing Distance	650mm to Infinity
Microwave Unit	2.45 GHz, 3000W	Optical Resolution	≥ 300:1

* Model MA2S-C-SF Santa Cruz, CA, USA

(a)

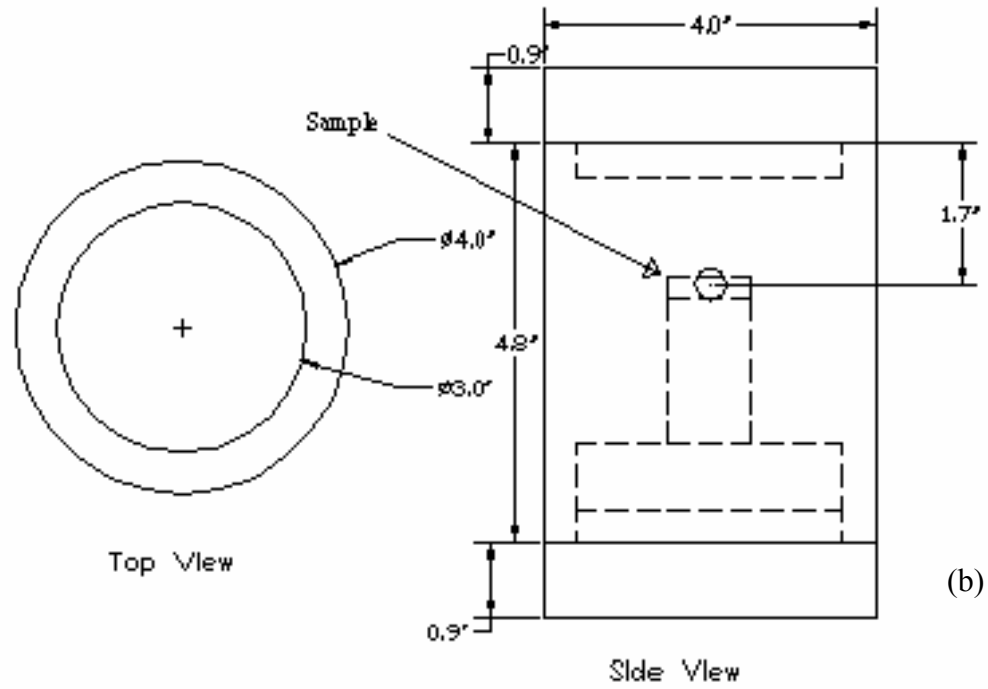

(b)

Figure III-2. (a) Insulation box, susceptors and the sample.
(b) Schematic drawing of the insulation box.

Table III-II Power-Time Profile

Time	Power	Command Voltage
5 min.	20 %	1.46
5 min.	25 %	1.84
5 min.	30 %	2.19
25 min.	33 %	2.44

Nine locations inside the microwave chamber were studied (Fig. III-3). The box, which had only one sample inside during each run, was placed onto marked spots, on the table, inside the MW chamber, and a specific power-time profile was applied (Table III-II).

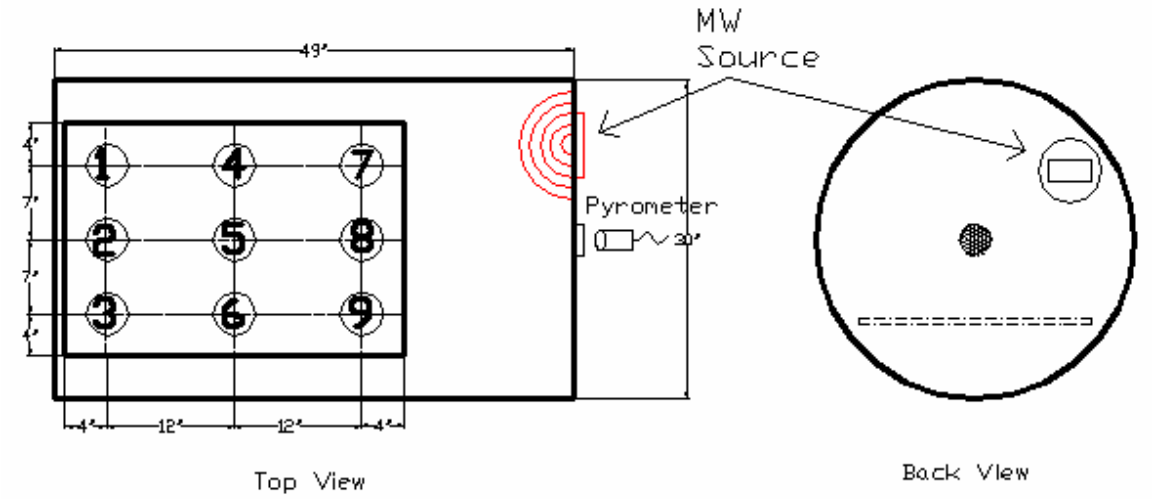

Figure III-3. Schematic drawing of CPI Autowave microwave furnace.

Densities of the samples, which were sintered at different positions, were measured using the Archimedes method.

Another set of experiments was used to study the effect of temperature and dwell times on the sintered densities of different samples. Tosoh TZ-3YS zirconia and Baikowski Alumina samples were used for these experiments; and they were prepared in accordance with the previously described procedure. For the zirconia materials three different temperatures and four different dwell times were employed (Table III-IIIa). For Alumina a smaller test matrix, with three different temperatures and three different times was used (Table III-IIIb).

Table III-III Temperature & Dwell Time Matrix of Zirconia (a) and Alumina (b).

Zirconia	1440 °C	1460 °C	1480 °C
0 min.	Z11	Z12	Z13
5 min.	Z21	Z22	Z23
10 min.	Z31	Z32	Z33
15 min.	Z41	Z42	Z43

a

Alumina	1480 °C	1500 °C	1520 °C
10 min.		A12	
15 min.	A21	A22	A23
20 min.		A32	

b

After the density measurements were made, samples were cut in half and their cross sectional areas were polished using Automet polisher (30, 15, 6 and 1 micron diamond suspensions respectively were used at 10 min. intervals each.). Vickers hardnesses were measured on the polished surfaces of each sample at 9 points (3 near the top surface, 3 from center and 3 near the bottom). Hardness tester Leco* was used for hardness measurements. Following the hardness measurements, samples were thermally etched at 1000 °C for zirconia and 1440 °C for alumina. Etched sample surfaces were examined under SEM 510 (Philips) and micrographs of the grains were taken. Those micrographs were digitally filtered by using the HighPass filter option of PhotoShop software to get a better view of grain boundaries. By using a pen, the printed micrographs of grain boundaries were outlined and scanned for image analysis. Image Pro software was used for the grain size analysis. Grain size distributions were based upon area of the grains. Additional details of etching and grain size measurement are provided in the results and discussions.

* Model V-100-A2 St.Joseph, MI, USA

C. Microwave and Conventional Sintering of SGP Printed Samples

Alumina slurries with different compositions were prepared at the Metrix Composites Inc.* and 1" diameter disks were printed. SGP-technique was used for the printing process. Table III-IV shows the compositions of slurries used in this study. SGP printed disks were then sintered using microwave and conventional methods. The CPI Autowave (microwave) and the Thermolyne High Temperature Tube Furnace (conventional) were used for sintering. Time and temperature profiles for both microwave and conventional sintering was 15 min. dwell time at 1500°C.

Table III-IV Compositions of Slurries Used in SGP printing.†

	B1	*B2*	*B3*
Amount (g)			
Darvan 821A	8.28	5.84	11.69
Alumina Powder	974.11	974.11	974.11
Sodium Citrate	0.39	0.39	0.39
Water	200.25	200.25	200.25
Alginate (2 wt% solution)	48.30	48.30	48.30
Percentage (%)			
Darvan Content	0.85	0.60	1.20
Solid Volume Loading	55	55	55
Alginate Content	0.4	0.4	0.4

* Utica, NY, USA

† Darvan content expressed in terms of weight percentage based on solid weight. Solid volume loading expressed in terms of volume percentage based on total slurry volume. Alginate content expressed in terms of weight percentage based on water weight. Alginate solution added to the slurry just before the printing and none of the percentage calculations include alginate solution

D. Density Measurements (Archimedes')

Densities of sintered samples are measured by Archimedes method (ASTM standard designation C 20 – 97). Archimedes method is a useful and accurate method for samples which have irregular shapes. Archimedes method is based upon the fact that the amount of the weight decreases when an object immersed in a liquid. This effect is equal to the weight of the volume of the liquid that of the object displaced. Therefore, the bulk density of the object can be calculated in accordance with Equation 8. Equation 9 and Equation 10 illustrate the pore volume and porosity calculations, respectively.

$$Density = \frac{D}{W - S} x\rho_{water} \qquad (8)$$

$$Pore \quad Volume = (W - D)x\rho_{water} \qquad (9)$$

$$Porosity = [(W - D)/(W - S)]x\rho_{water}x100 \qquad (10)$$

Where, D is the dry weight, W is the saturated weight and S is the suspended weight in water.

The sintered samples were submerged in boiling de-ionized water for 2 hours and allow to cool to room temperature. They remained submerged for a minimum of an additional 12 hours. Thereafter their suspended weights and their saturated weights were measured with AND (HA-202M) digital balance.

E. Sample Characterization

Samples were cut into 2 pieces and molded into bakelite. SiC papers with grit sizes of 240, 320 and 400 respectively were used to rough grind the zirconia samples. Alumina samples were rough ground with a diamond disk. Fine polishing done with Buehler[*] Ecomet 3 polisher using 30 μm, 15 μm, 6 μm, 1 μm diamond slurries respectively. Afterwards samples extracted out of mold by cutting them out, and the samples were thermally etched in Thermolyne[†] high temperature furnace. Zirconia

[*] Lake Bluff, IL, USA

[†] Dubuque, Iowa, USA

samples were thermally etched at 1000°C and alumina samples at 1440°C for 18 min. Etched samples were examined under SEM* at 25kV and with a spot size of 50 nm. Images were taken at a resolution of 2K x 2K. Grain boundaries on those images were outlined and grain sizes were calculated from outlined images by using ImagePro (Media Cybernatics) software. More details of sample preparation and characterization is provided in results and discussions.

* Model 510 Philips

IV RESULTS AND DISCUSSIONS

A. Slurry Preparation and Characterization

1. Shear Thinning Effect

The leveling of the slurry in Selective Gelation Method (SGP) is very similar to a tape casting process where a doctor-blade is used to form a tape of specific thickness. Shear thinning behaviour of the slurry is very useful for getting a smooth levelling process. When the doctor-blade moves, the slurry between doctor-blade and substrate (carrier tape) surface encounters a shear force. A shear thinning behaviour of the slurry momentarily decreases the viscosity and makes the levelling process easy. After doctor-blade past away from that point, shear force will disappear and the viscosity of the slurry will increase again. Increased viscosity helps the slurry to maintain a uniform layer thickness. Fig. IV-1 shows the shear-thinning behaviour of the alumina slurries at different Darvan concentrations. All slurries had 55 vol% powder content. The effect of shear force on the viscosity was much higher than the effect of Darvan. Speed of the doctor blade in actual printing process was ~10mm/sec and the layer thickness was 150μm. According to this data shear rate was equal to 64/sec.

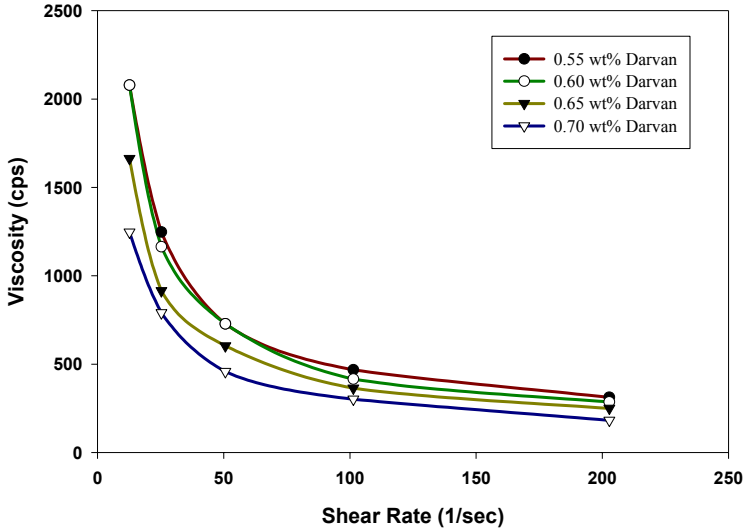

Figure IV-1. Viscosity change as a function of shear rate.
(55 vol% alumina and no alginate)

2. Effect of Darvan on Viscosity

A well dispersed slurry has several advantages. For example, the slurry can be easily dispense on to build table. Low viscosities are needed and this can be achieved by having a good dispersion. Darvan 821A is used for dispersing the slurries of selective gelation printing. Fig. IV-2 shows the effect of Darvan content on viscosity of the slurry. It is obvious from the results that a Darvan concentration of ~0.7 to 1.0% needed to achieve the optimum (low) viscosity.

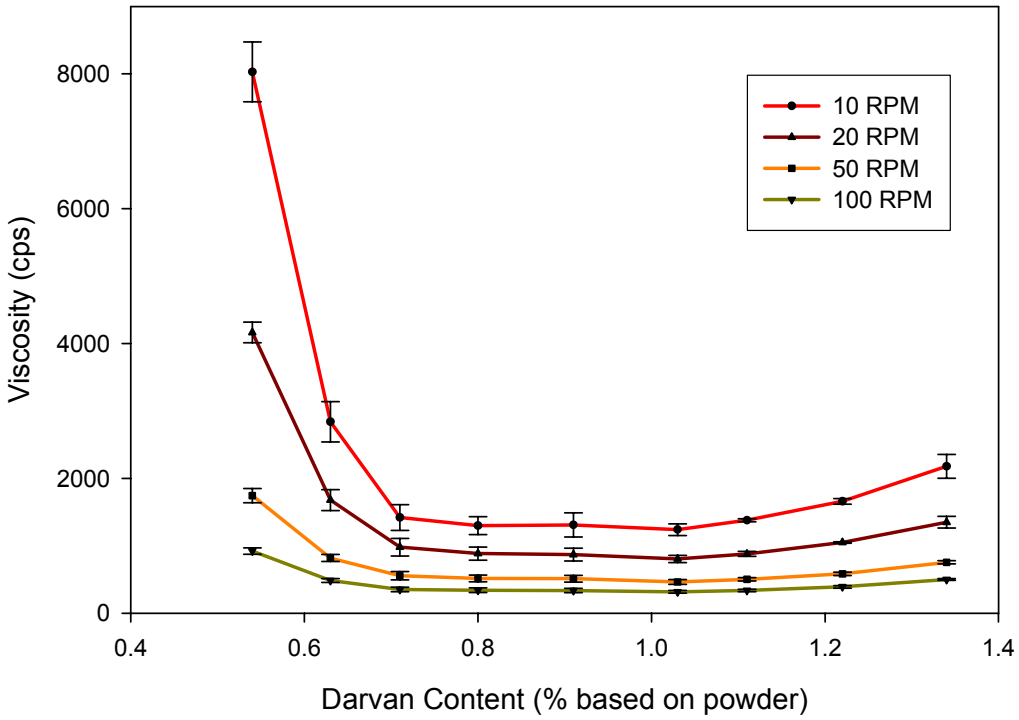

Figure IV-2. Viscosity change as a function of dispersant content.
(52 vol% alumina and no alginate)

At low levels of dispersant (<0.7%), agglomerates become smaller compared to the slurry without any dispersant. But there are still agglomerates and the viscosity is still high, due to interparticle bridging structures. At the minimum viscosity range, all particles are evenly dispersed and the system reaches its maximum mobility. At high solid contents, as in this slurry (52 vol%), a significant portion of the liquid was adsorbed as shells about the dispersed particles and most of this water was immobilized as a result

of the hydration of the counter ions in the dispersion. When the dispersant content was increased to higher values, beyond the minimum viscosity range (0.7-1.0%), more ionic material goes into the solution phase. This immobilizes additional liquid from the fluid phase and increases the viscosity of the system. The other reason for increased viscosity is the bridging of polymer chains between particles.

3. Effect of Solid Loading on Viscosity

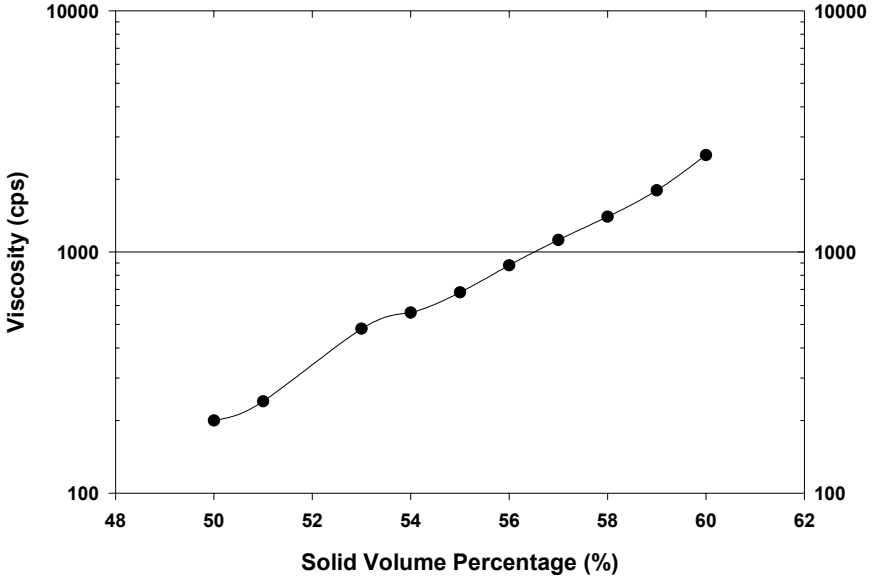

(a)

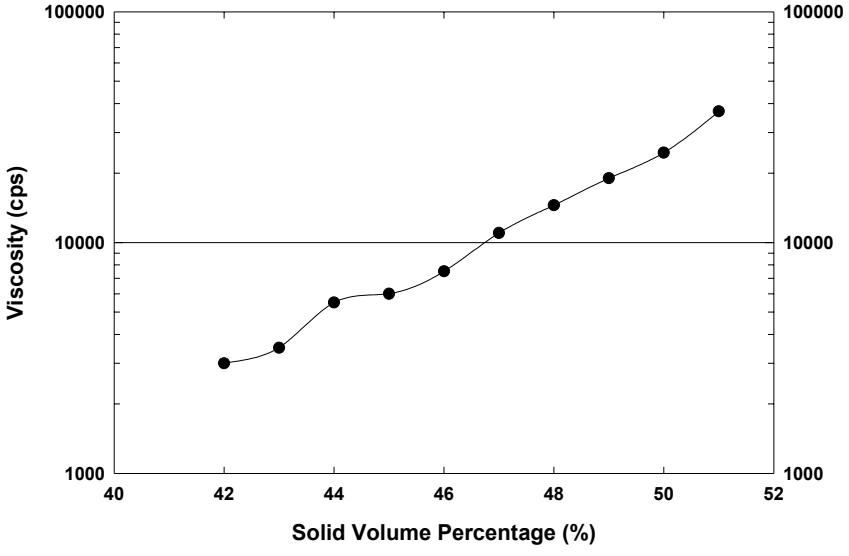

(b)

Figure IV-3. Viscosity change of alumina (a) and zirconia (b) as a function of solid content.

The viscosity of the zirconia slurry was much higher than the viscosity of the alumina slurry even at lower solid contents. Most probably this behaviour was caused by the larger average particle size (diameter) of the alumina powder of 0.35 μm whereas it was 0.035 μm for zirconia powder. Surfaces of the fine powders immobilize the water by structural entrapment at lower solid contents. Also, weak structuring forces caused by dispersant adsorbed particles, create solid bridge networks and trap the liquid inside.[16] Those two effects, increases the viscosity of the slurries of fine particles and even at low solid contents, the viscosity of the zirconia slurry is relatively high.

4. Zeta Potential Measurements

Another important factor in slurry preparation is the suspension stability. Although the printing time is not too long (it can take about 2 hour to 12 hour depending upon the specifics of the sample geometry and printing conditions) the slurry should stay homogeneous over that "printing time". This can only be achieved by having sufficient suspension stability. Zeta-potential (ξ) is widely used as an indicator of the stability, it indicates the repulsive part of the particle interaction. Slurries prepared at pH values close to isoelectric point (IEP) may flocculate relatively faster compared to slurries prepared at pH values away from the IEP. Repulsion may not be sufficient to overcome the van der Waals attraction at pH values close to IEP. To get good repulsion, slurries should be prepared in a region where the zeta-potential is $> \pm 40$ to 50 mV. As prepared pH's of both alumina and zirconia slurries were ~9, which is a suitable region for both materials. (Fig. IV-4).

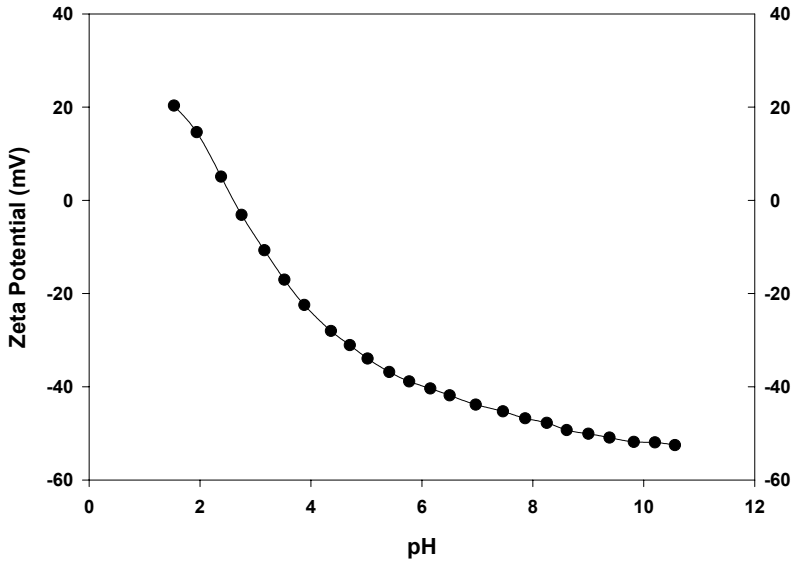

(a)

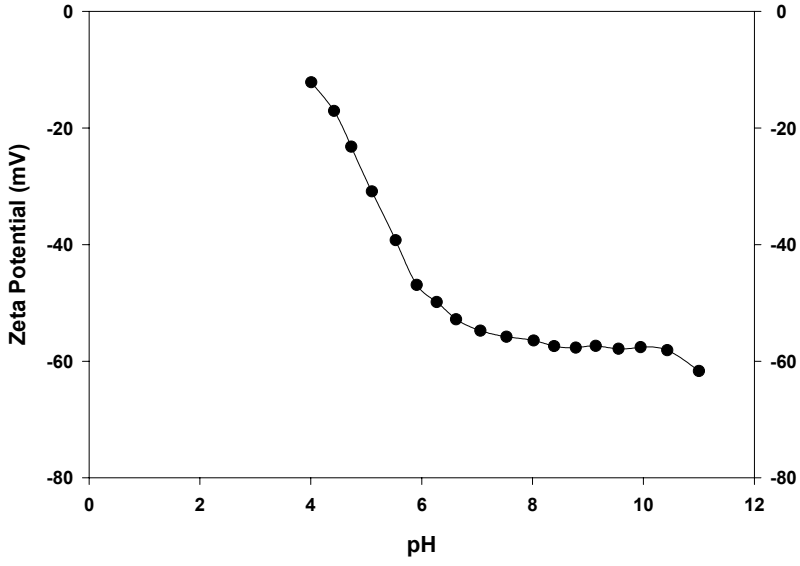

(b)

Figure IV-4. Zeta-potential change of alumina (a) and zirconia (b) as a function of pH.

B. Mapping and Optimization of MW sintering

1. Mapping of the CPI Autowave Microwave Furnace

Microwave furnaces, especially untuned ones, do not have a uniform electric and magnetic field distribution inside the cavity and thus, resulting in non-uniform heating characteristics. This is mostly because of the wave behaviour of microwaves. Their wavelengths range from 1 m to 1 mm. They can be transmitted, absorbed or reflected depend on the material type. They also show cancellation and reinforcement interference, this makes the microwave distribution inside the cavity non-uniform.

In this study, cavity homogeneity was examined by setting up 9 test spots inside the cavity (Fig. III-3). Tests were performed by sintering 1" diameter pressed TZ-3YS zirconia discs and applying the same power-time profile (Table III-II) for each of the 9 positions. Table IV-I shows the densities observed on each position. Theoretical density 6.06 gr/cm^3 was assumed for zirconia.

Table IV-I Densities of the Zirconia Samples*

1 96.3%	**4** 93.9%	**7** 92.0% 90.9%
2 97.8% 98.9%	**5** 95.2% 94.5%	**8** 95.8%
3 98.9% 98.0%	**6** 94.4%	**9** 95.7%

* Samples sintered at different positions with the same power profile.

There was a significant density difference (~8%) between position 7 and position 3. This demonstrated the nonuniformity of the cavity. Cancellation and reinforcement interference of the microwaves creates hot (reinforcement) and cold (cancellation) points inside the cavity. Figure IV-5 shows the mapping of the CPI Autowave cavity according to the measured densities of the zirconia samples. The shown response surface was quadratic equation and the corresponding R and R^2 values were 0.924 and 0.854, respectively.

Temperature data could not be taken for all the spots, because the 4 mm thick microwave grid in front of the pyrometer window did not allow angled views for the pyrometer when pointed at some of the corner positions (see Fig. IV-6). Minimum focus distance of the pyrometer was 650mm so positions 5 and 8 was out of range for focusing and they did not give accurate temperature readings. As a result, mapping is done based on theoretical densities measured with Archimedes method. The maximum temperature at position 2 with this power profile (Table III-II) was around 1470°C. Intentionally a power profile was used which did not result in >99.9% theoretical density. A lower temperature (power profile) was chosen in order to see the density variations. If the temperature would be too high all the samples will have theoretical densities close to 100% and if it would be too low samples would not sinter at all. Position 2 is used for temperature reading in further studies since it was the best point which gives accurate results.

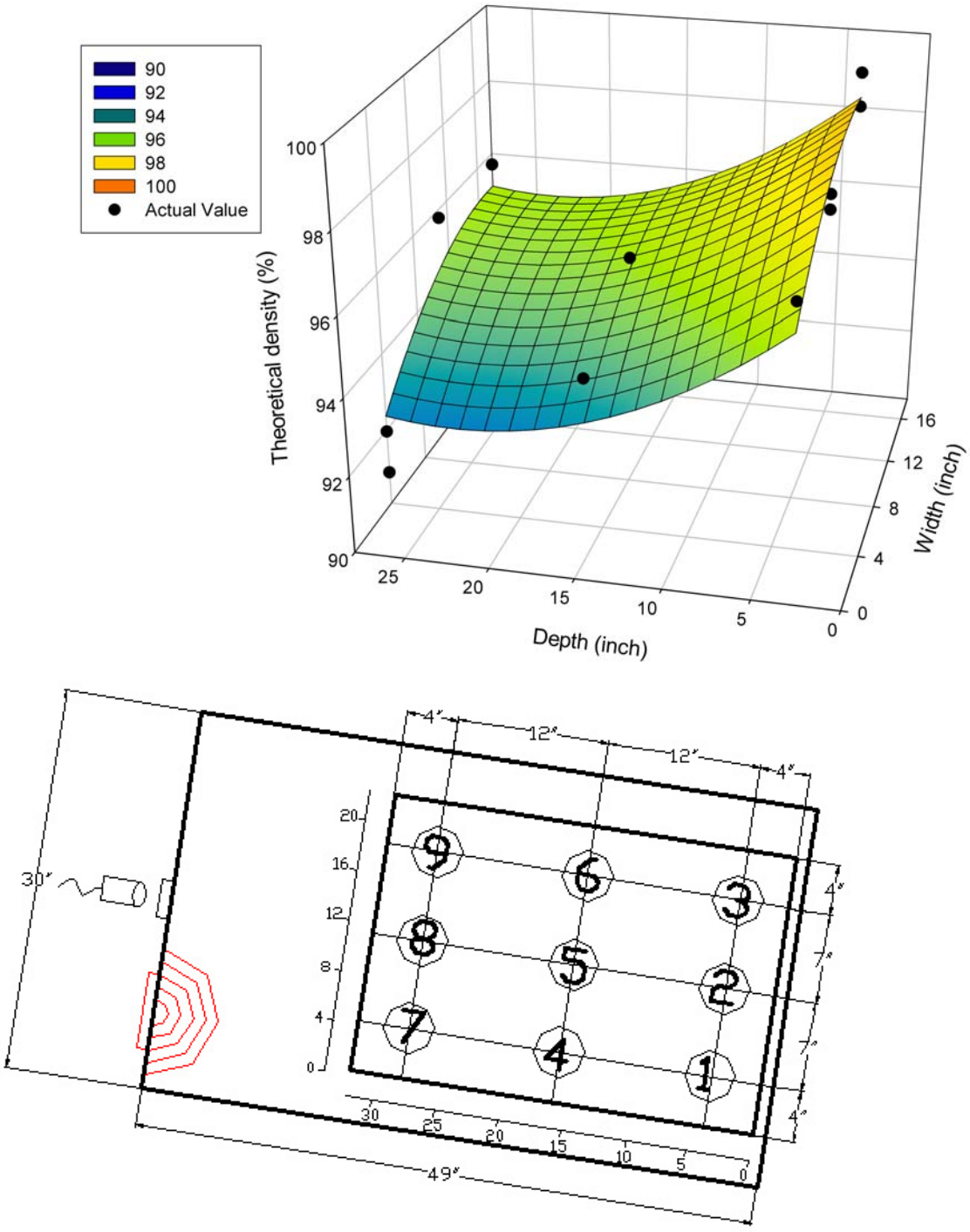

Figure IV-5. Mapping of CPI Autowave microwave furnace cavity.

Figure IV-6. Pyrometer setup.

2. Temperature and Time Effects on Sintered Density During MW Sintering

Effects of sintering time and temperature was studied by using both alumina and zirconia pellets. Table IV-II & IV-III show the measured theoretical densities, hardness and porosity of zirconia and alumina samples at corresponding hold times and temperatures. All measurements in this part of the study were carried out on position 2 to get the most accurate temperature readings. 6.06 g/cm^3 and 3.96g/cm^3 were assumed as the theoretical density for zirconia and alumina, respectively.

Table IV-II Characterization Values of Microwave Sintered Zirconia Samples

Sample # ***Hardness (VHN)*** ***Theoretical Density (Second TD)**** ***Porosity***		Sintering Temperature		
		1440 °C	1460 °C	1480 °C
Dwell Time	0 min.	Z11 **608** ±12 **82.2%** **(81.8%)** **17.8%**	Z12 **738** ±81 **85.4%** **(85.7%)** **14.6%**	Z13 **888** ±12 **91.3%** **(91.2%)** **8.7%**
	5 min.	Z21 **1063** ±13 **95.0%** **(94.4%)** **5.0%**	Z22 **1207** ±31 **95.7%** **(96.0%)** **4.3%**	Z23 **1213** ±25 **97.0%** **(98.6%)** **3.0%**
	10 min.	Z31 **1123** ±23 **96.3%** **(96.4%)** **3.7%**	Z32 **1278** ±39 **96.7%** **(96.1%)** **3.3%**	Z33 **1223** ±23 **98.6%** **(99.0%)** **1.4%**
	15 min.	Z41 **1142** ±13 **95.9%** **(95.6%)** **4.1%**	Z42 **1284** ±18 **96.6%** **(96.2%)** **3.4%**	Z43 **1264** ±16 **99.2%** **(98.0%)** **0.8%**

* Theoretical densities of the samples measured twice and the results of second measurement shown in parentheses.

Table IV-III Characterization Values of Microwave Sintered Alumina Samples*

Sample # ***Hardness (VHN)*** ***Theoretical Density (Second TD)*** ***Porosity***		Sintering Temperature		
		1480 °C	1500 °C	1520 °C
Dwell Time	10 min.		A12 **1650** ±62 **97.7%** **(96.8%)** **2.3%**	
	15 min.	A21 **1613** ±46 **97.9%** **(96.7%)** **2.1%**	A22 **1690** ±31 **98.3%** **(98.8%)** **1.7%**	A23 **1701** ±40 **99.4%** **(99.7%)** **0.6%**
	20 min.		A32 **1718** ±44 **99.0%** **(98.0%)** **1.0%**	

As the density of a sample increased its hardness increased as expected. However, in the zirconia matrix there is a slight decrease in the hardness at high temperatures (1480°C). According to Hall-Petch type relationship (Equation 11), hardness decreases with increasing grain size. Up to a certain point high temperature helps to decrease porosity and this increases the hardness, but after the porosity reaches a low enough value, the effect of increased grain size, caused by prolonged sintering holds at high temperatures, starts to dominate and decreases the hardness.

$$H = H_O + k' d^{-1/2} \qquad (11)$$

* Theoretical densities of the samples measured twice and the results of second measurement shown in parentheses.

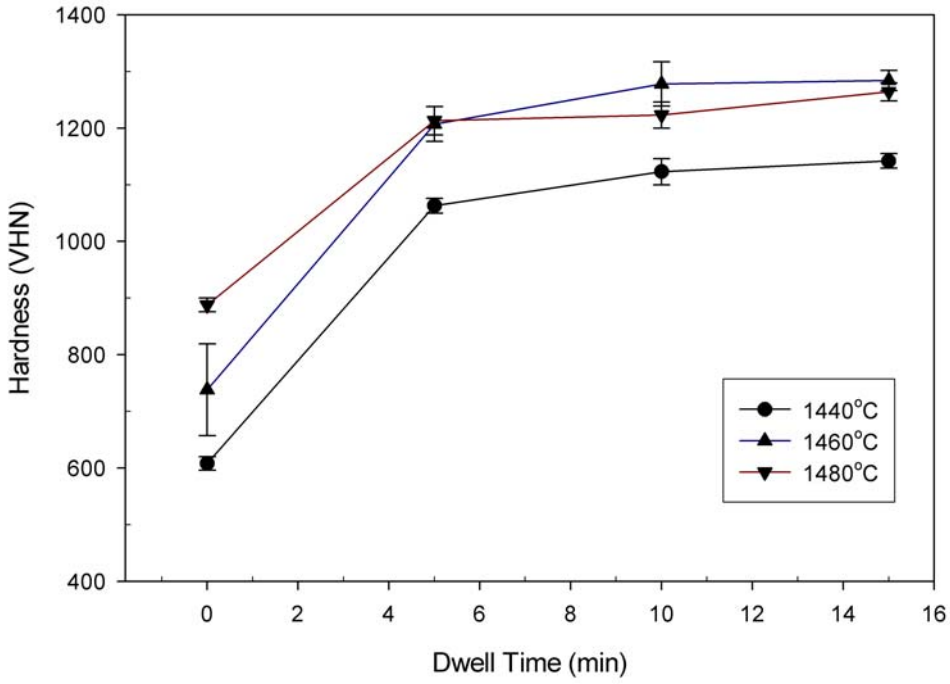

Figure IV-7. Hardness values of the microwave sintered zirconia samples vs. dwell time. (see Table IV-II)

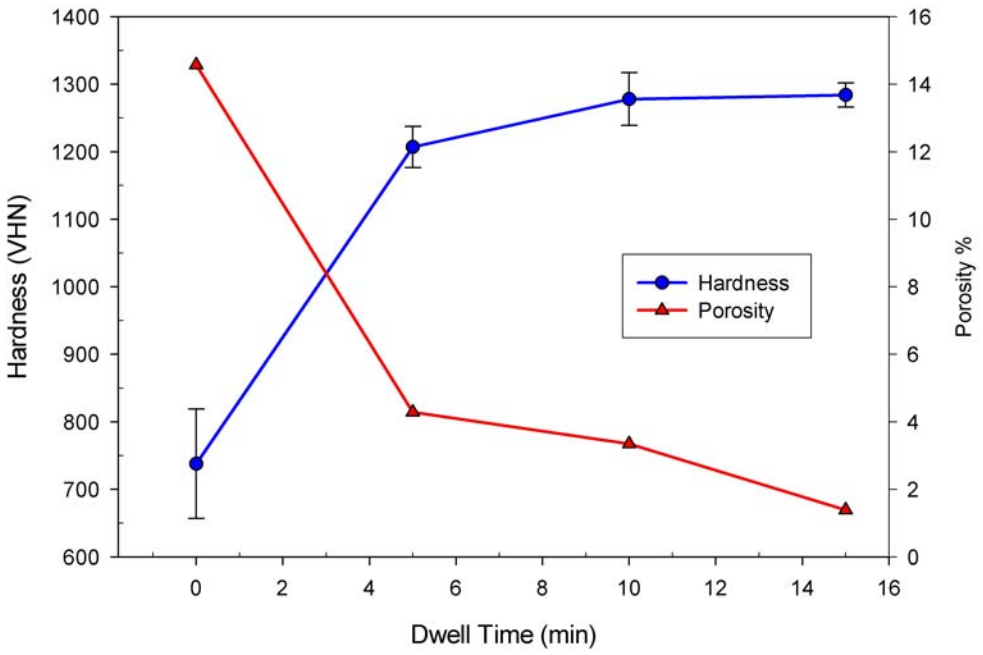

Figure IV-8. Hardness and porosity of the microwave sintered zirconia samples at 1460°C. (see Table IV-II)

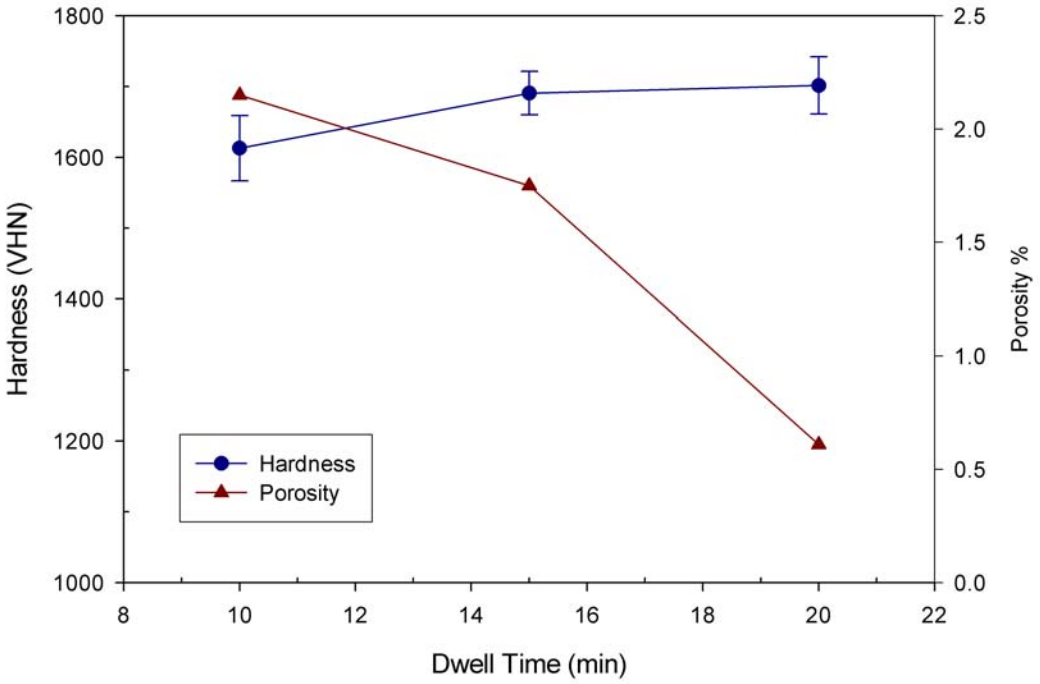

Figure IV-9. Hardness and porosity of the microwave sintered alumina samples at 1500°C. (see Table IV-III)

3. Heat-up Rate Comparison (MW vs Conventional)

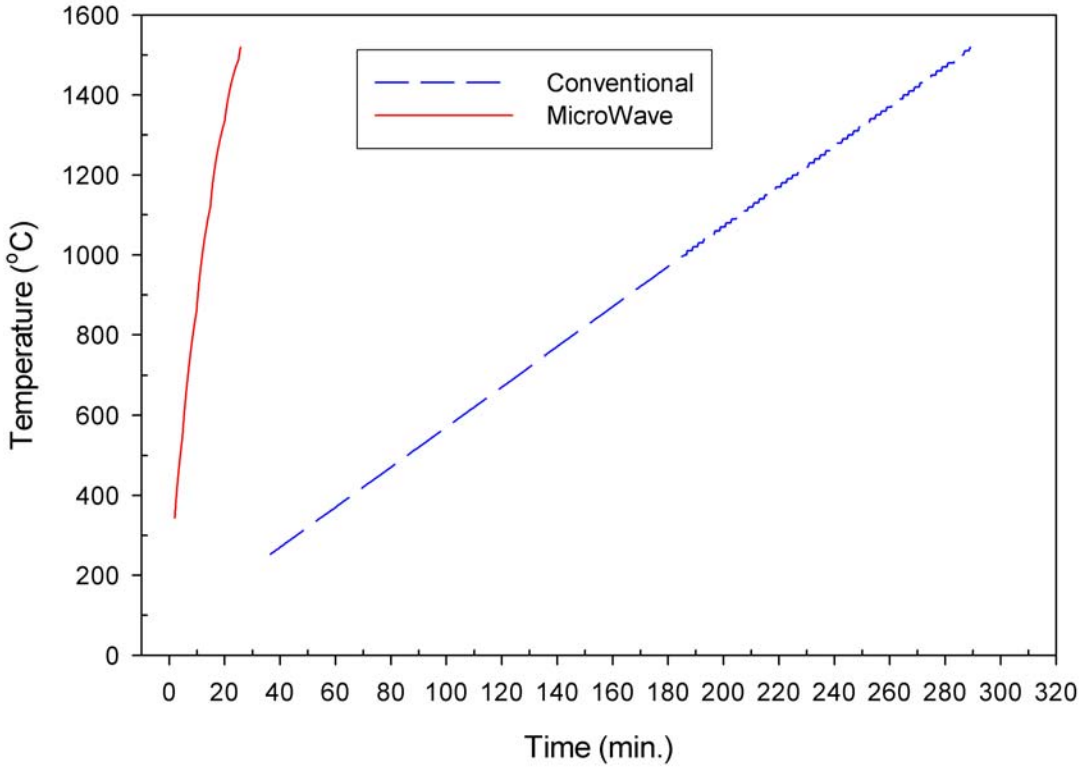

Figure IV-10. Heat-up rates of conventional and MW sintering.

Table IV-IV. Heat-up Rates of Microwave and Conventional Sintering.

Temperature Range (°C)	**MW**	**Conventional**
350-500	78 °C/min	5 °C/min
500-1000	63 °C/min	5 °C/min
1000-1500	38 °C/min	5 °C/min

The same power profile as shown in Table III-II was used for the microwave experiment. The heating rate was not constant for microwave sintering because there was not a control feedback between the pyrometer and MW-power control computer. All power controlling was done manually. As the temperature increased more power was required to continue heating at a constant rate, however the mw power was not enough to hold the rate constant at temperatures above 1000°C. However, it should be possible to achieve a "constant" heat-up rate if there were a direct feedback between pyrometer and the mw-power controller. In the conventional heat-up, rate was controlled with the furnace power controller and kept constant at 5°C/min. (Fig. IV-10)

As mentioned earlier in the literature survey, microwave energy penetrates the material to be processed and thus heat is generated rapidly throughout the entire sample ("volume heating"). In conventional heating, the outside of the material heats up first and then the heat travels inwards by thermal conduction. The energy transferred depends on the thermal conductivity coefficient of the material and the temperature difference between outside and inside of the material. If the heating rate is increased too much there will be problems like large temperature gradients within the materials. Therefore, heat-up rates should be relatively slow in conventional heating.

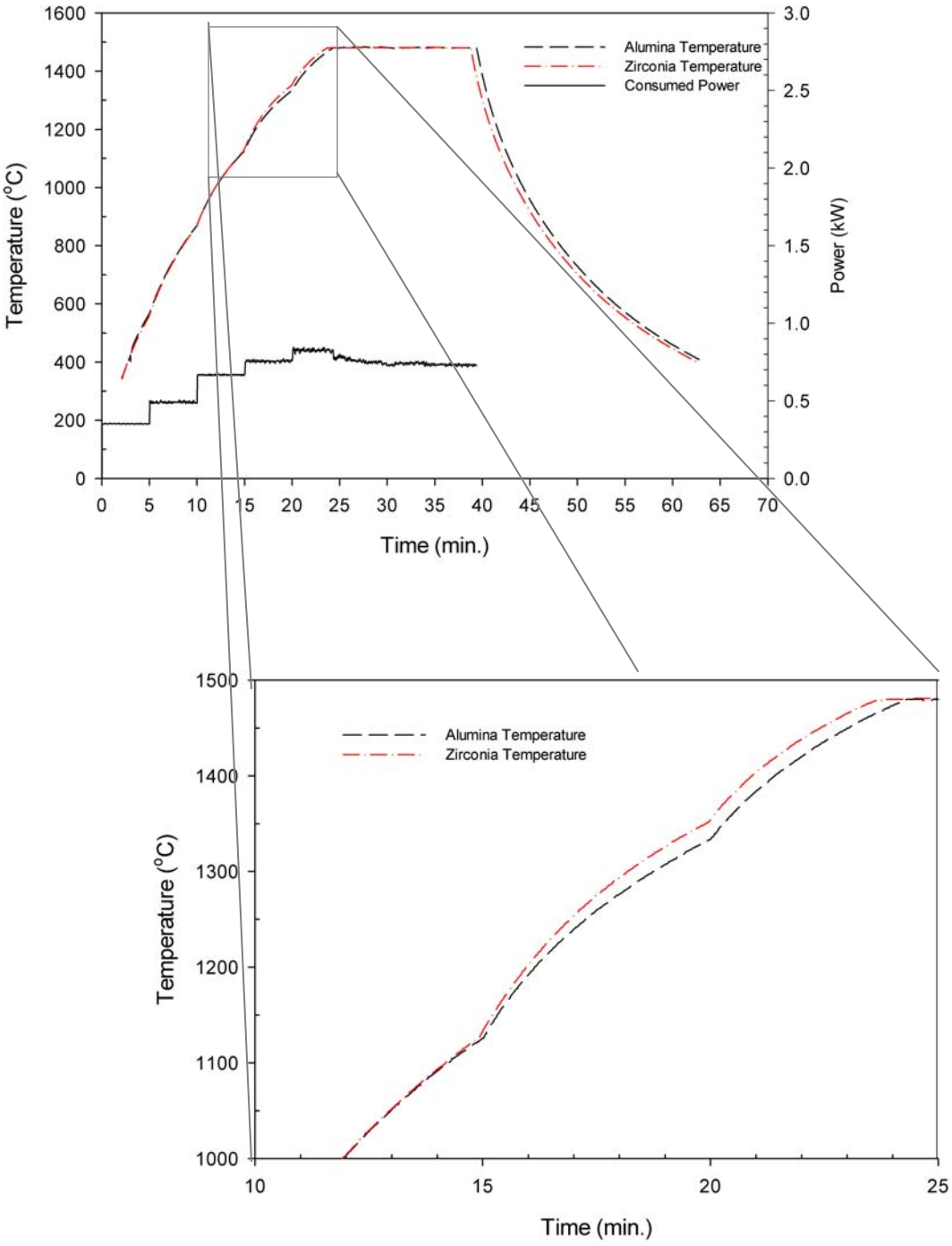

Figure IV-11. Heating curves of zirconia and alumina samples.

Figure IV-11 shows the heating of zirconia and alumina samples. At high temperatures zirconia has a slightly higher heat-up rate compared to alumina. As mentioned in the literature survey, heat-up of materials depends on their loss mechanisms and those loss mechanisms are all combined together in the loss parameter, $\varepsilon''_{eff.}$ But usually the loss tangent is used to describe losses. When microwaves penetrate and propagate through the material, free and bound charges are affected by microwaves and dipoles attempt t move. As a result, resistance occurs across this movement of charges and dipoles. Resistance comes from the inertial, elastic and frictional forces and this causes losses. So, heat depends on the losses of the material and as mentioned above usually loss tangent shows the amount of losses. Loss tangent of ceramic dielectric materials (Al_2O_3, Zr_2O_3, MnO, NiO…) increases with increasing temperature. Ho[25] reports that this increase related to the softening of intergranular, amorphous phases, which causes an increase in the local conductivity σ. And as can be seen from Equation 6 an increase in σ, increases the loss tangent. Zirconia has a higher loss tangent value at high temperatures than does alumina. And at higher temperatures zirconia couples with microwaves more efficiently than alumina do. This results in a faster sample temperature increase for zirconia when compared with the alumina system. Fig. IV-11 shows this difference, for example after 20 min. run time, the temperature of the alumina sample was 20°C lower than for the analogous zirconia sample when using the same mw-power profile.

4. Optimization of Thermal Etching and Grain Size Measurement

Zirconia samples were polished without any specific problems. SiC papers (240, 320 and 400 grit) was used for rough grinding and then 30μm, 15μm, 6μm and 1 μm diamond solutions were applied for the fine polishing. However, for the alumina case, the hardness of SiC was too close to the hardness of alumina and this caused pitting of the sample during the initial grinding process (Fig. IV-12 (a)). So, a diamond wheel was used instead of SiC paper. Diamond has a higher hardness value than the alumina and was able to grind alumina without major pitting defects. (Fig. IV-12 (b)).

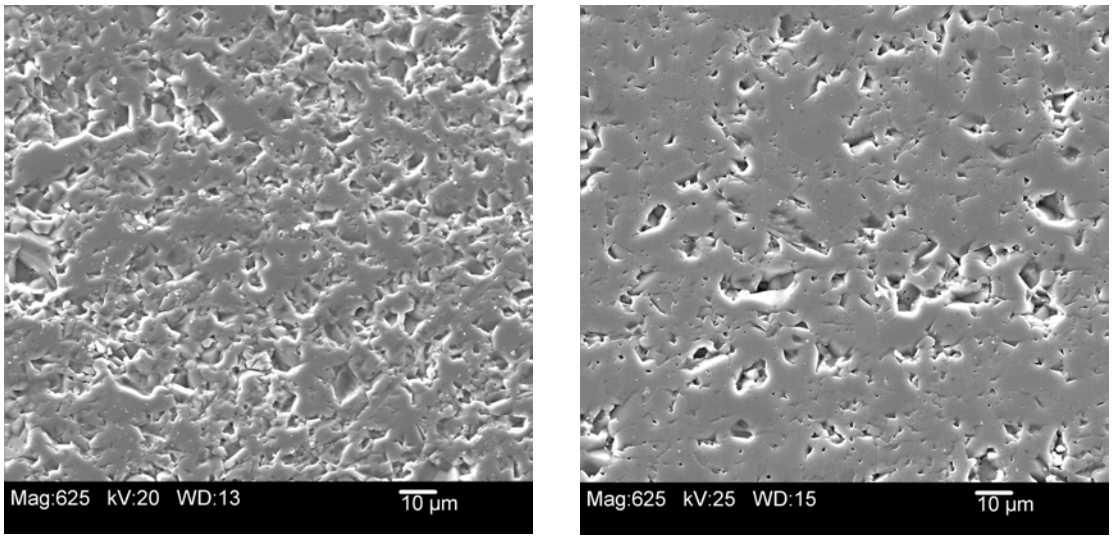

(a) (b)

Figure IV-12. (a) Alumina sample grinded with SiC paper, (b) Alumina sample grinded with diamond wheel.

As mentioned in the experimental procedure, sintered samples were first polished and then after the hardness measurement, thermally etched to measure the grain size. Thermal etching was the chosen method because ceramics are inert to many chemicals and this makes the chemical etching not a suitable method for the present materials. However one disadvantage of thermal etching is grain growth. Grain growth can occur during the thermal etching process. In general, dwell time of thermal etching is not as critical as the etching temperature.[27] Mass transportation mechanisms are active on the surface as well as under the surface of the samples during thermal etching. Thermal etching at high temperatures increases the rate of diffusion under the surface and this leads to grain growth. The driving force for grain growth is inversely proportional to the size of grains. So, especially for the fine grained samples the thermal etching temperature is very sensitive. In this study, different thermal etching temperatures for zirconia were tried and the lowest temperature which was just enough to see grain boundaries was chosen. The optimum thermal etching temperature profiles for the present zirconia samples and micrographs for the grain boundary sharpness shown in Figs. IV-13 through IV-15.

1450 °C

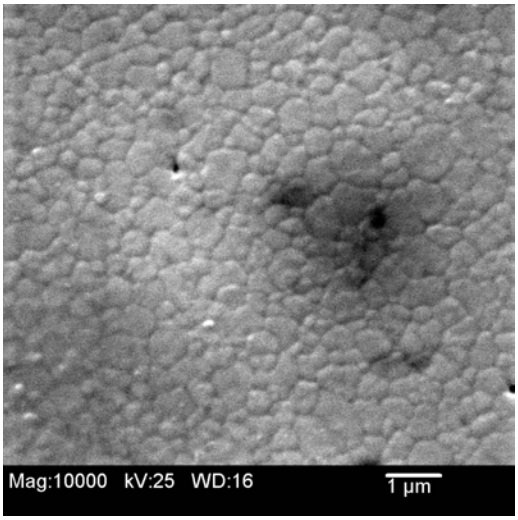

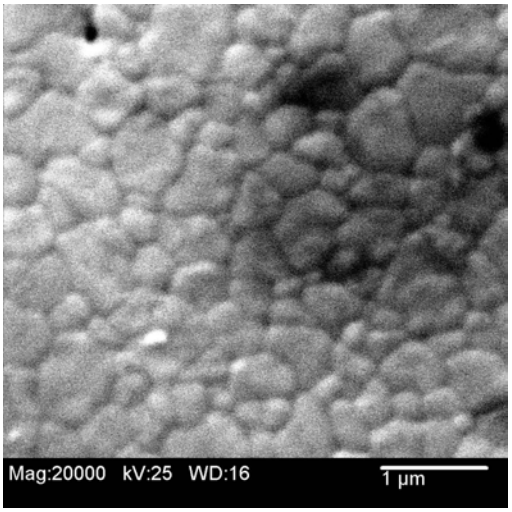

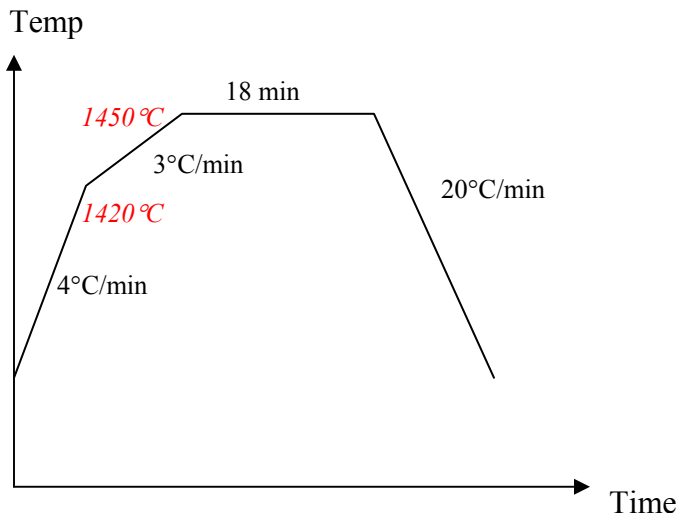

Figure IV-13. Thermal etching of zirconia at 1450°C.

1350°C

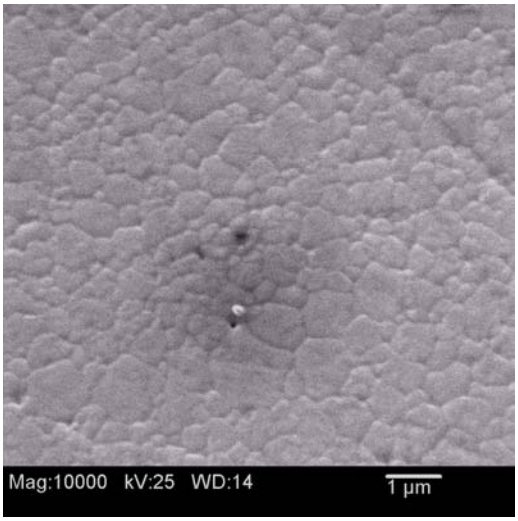

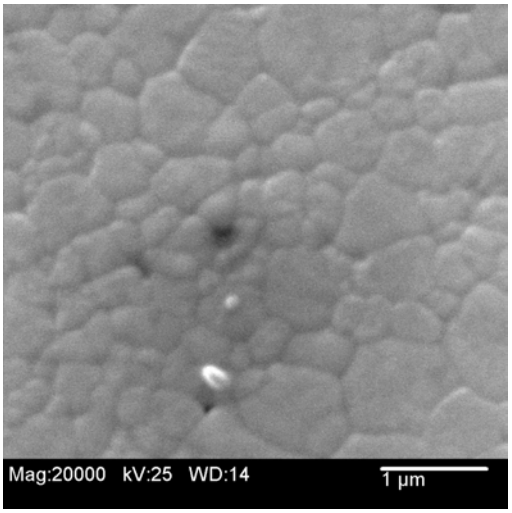

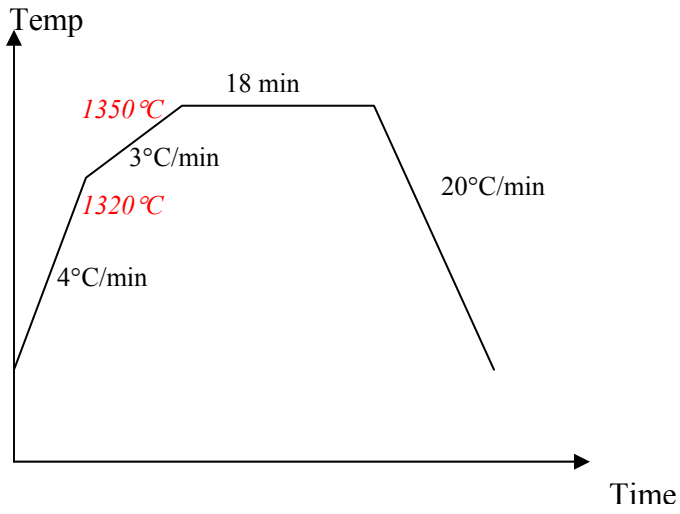

Figure IV-14. Thermal etching of zirconia at 1350°C.

1250°C

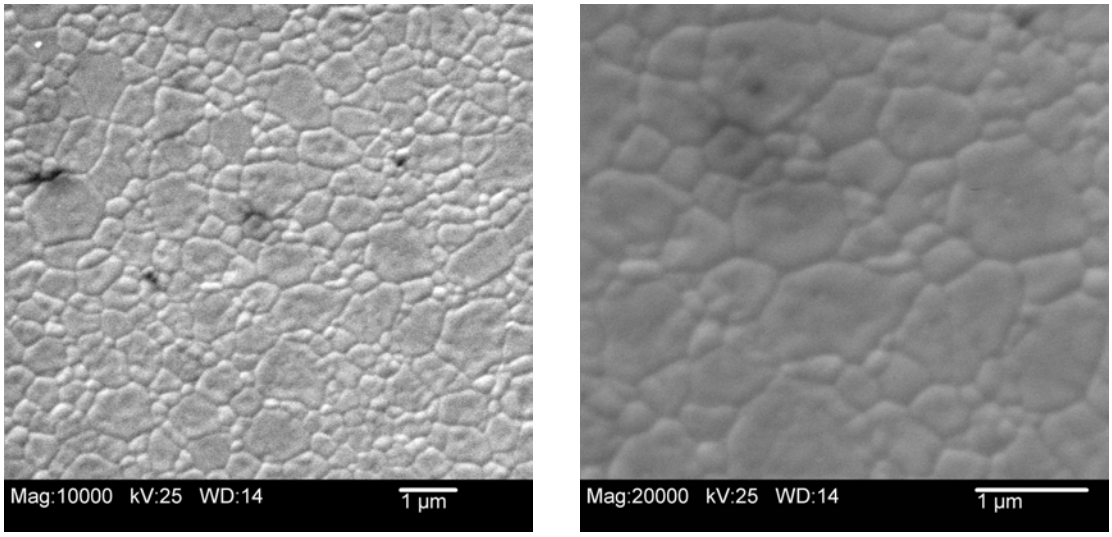

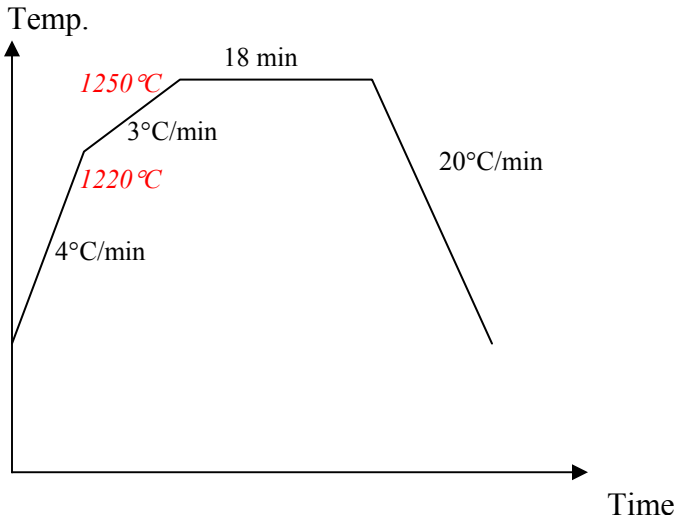

Figure IV-15. Thermal etching of zirconia at 1250°C.

After trying several temperature profiles, 1000°C was chosen for the thermal etching temperature of zirconia samples. 1000°C was the lowest temperature which was just sufficient to see the grain boundaries. Fig. IV-16 shows the results which were observed by thermal etching of zirconia sample at 1000°C. The sample shown in Fig. IV-16 is Z42.

As can be seen from Fig. IV-16 (a), micrograph taken by SEM was not clear enough to distinguish grain boundaries, even when brightness and contrast were adjusted. To make the grain boundaries more visible a special Adobe Photoshop filter called High Pass was used (Fig. IV-16 (b)).

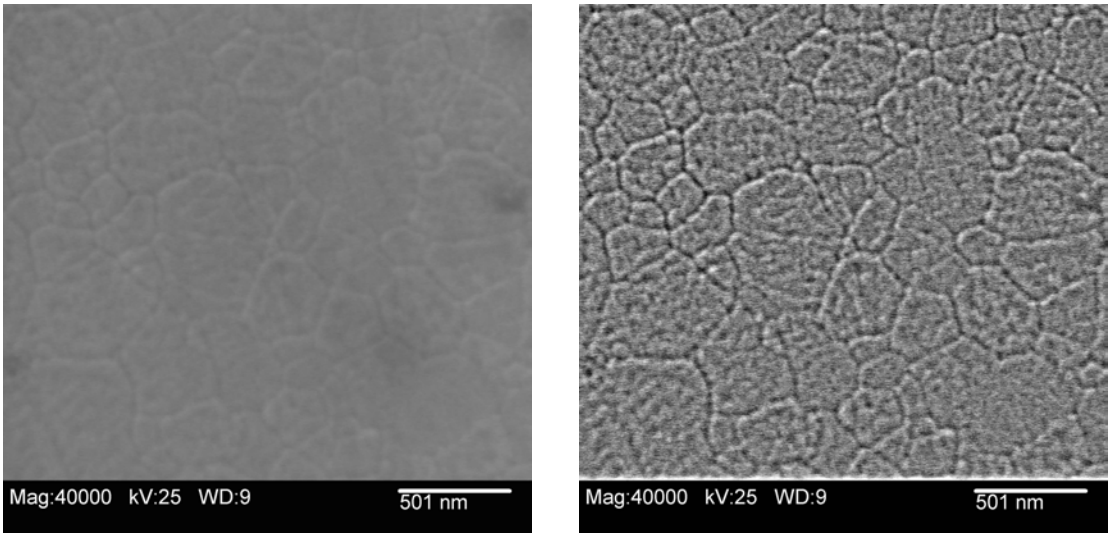

(a) (b)

Figure IV-16. SEM micrograph of sample Z42, thermal etched at 1000°C.
(a) Original SEM micrograph
(b) Computer enhanced picture

Afterwards image-Pro software was used for grain size analysis. A filtered micrograph which shows the grain boundaries (Fig. IV-17 (a)), is printed on a paper. Than all boundaries outlined with a pen (Fig. IV-17 (b)) and scanned (from the reverse side) (Fig. IV-17 (c)). The scanned image was then analyzed with Image-Pro software. Image-Pro calculates the area of each grain and creates an Excel spreadsheet.

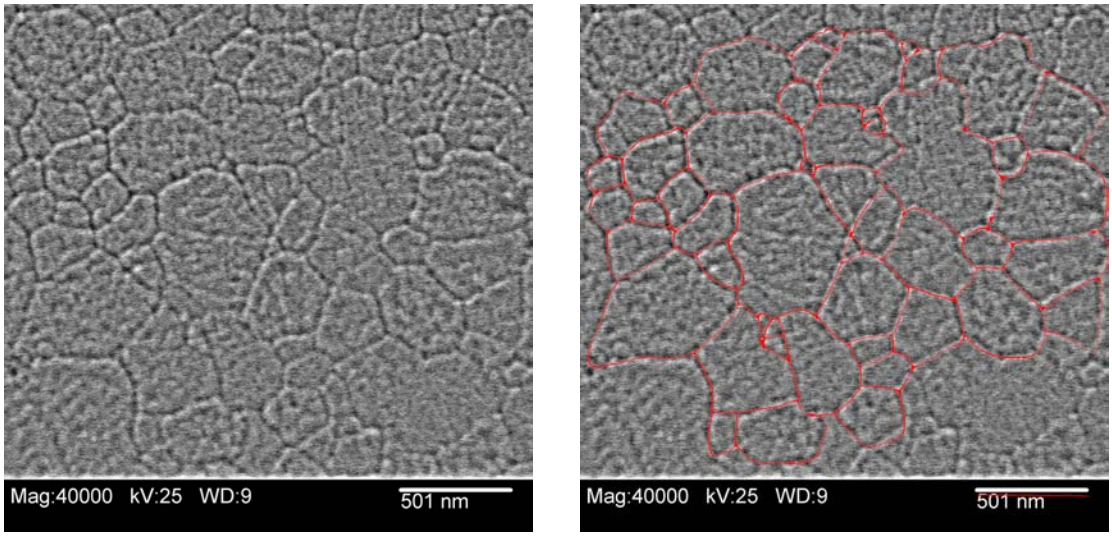

(a) (b)

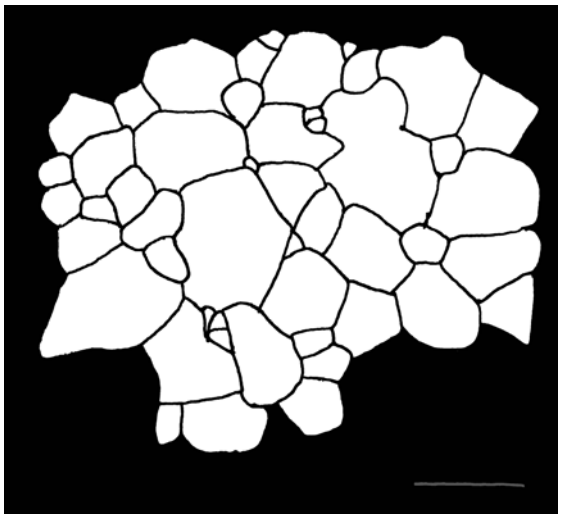

(c)

Figure IV-17. (a) Filtered SEM micrograph, (b) Outlined SEM micrograph, (c) Scanned image

5. Microstructure Characterization

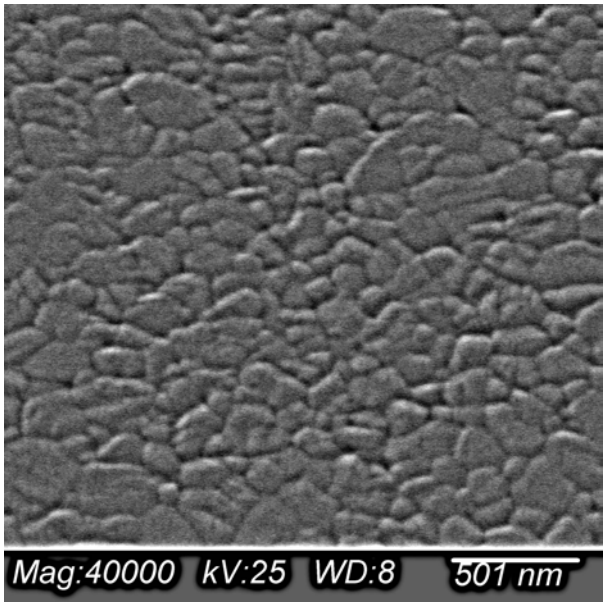

(a) Microwave sintered zirconia at 1440°C and 0 min. dwell time. (Sample # Z11)

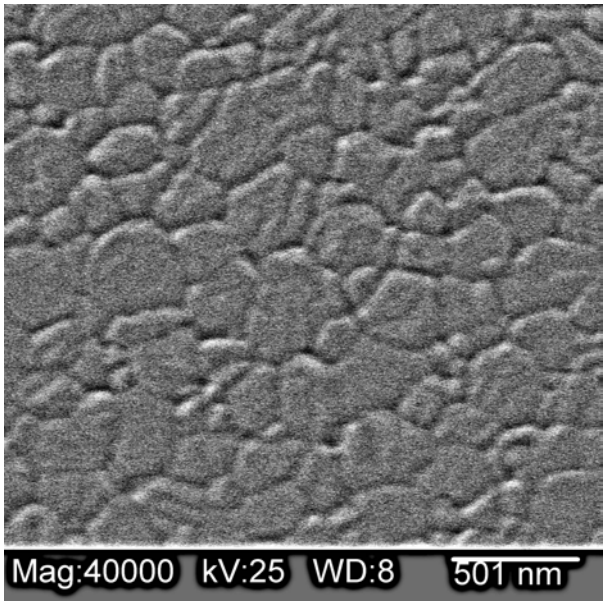

(b) Microwave sintered zirconia at 1440°C and 5 min. dwell time. (Sample # Z21)

Figure IV-18. a & b Micrographs of microwave sintered zirconia at 4 different dwell times and at 1440°C.*

* All micrographs are digitally filtered with PhotoShop High-Pass filter.

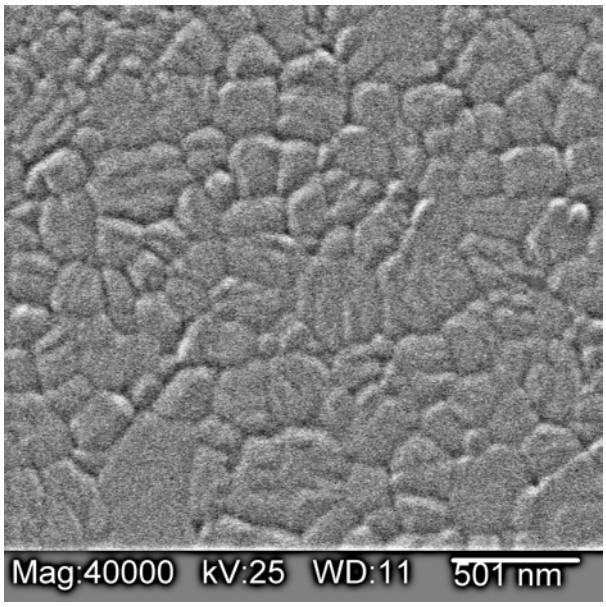

(c) Microwave sintered zirconia at 1440°C and 10 min. dwell time. (Sample # Z31)

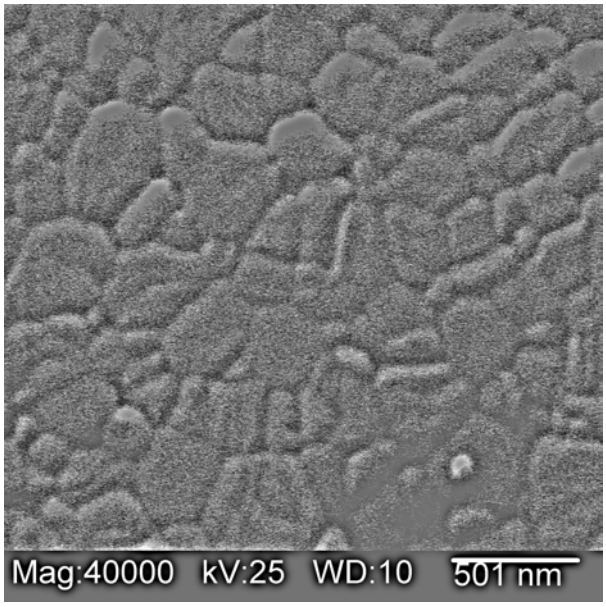

(d) Microwave sintered zirconia at 1440°C and 15 min. dwell time. (Sample # Z41)

Figure IV-18. c & d Micrographs of microwave sintered zirconia at 4 different dwell times and at 1440°C.*

* All micrographs are digitally filtered with PhotoShop High-Pass filter.

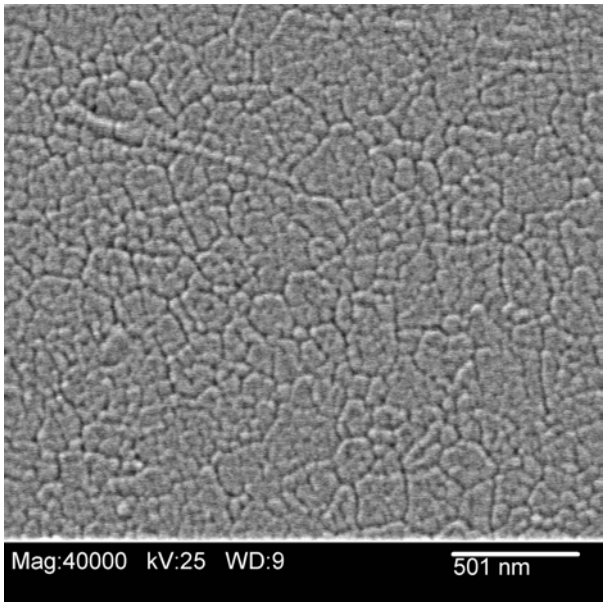

(a) Microwave sintered zirconia at 1460°C and 0 min. dwell time. (Sample # Z12)

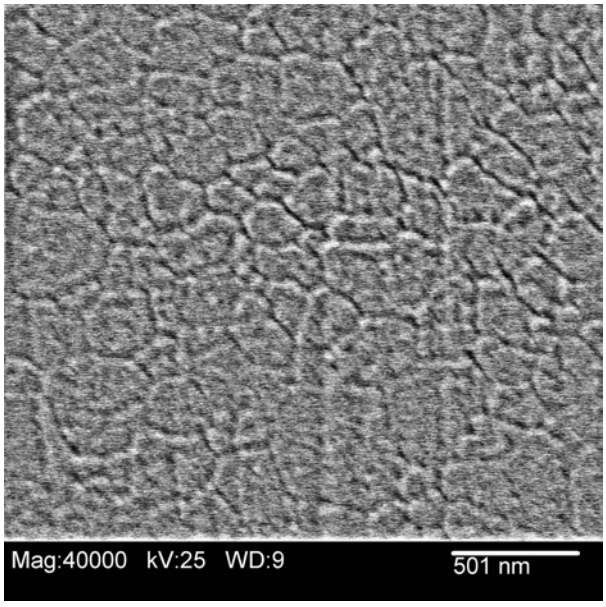

(b) Microwave sintered zirconia at 1460°C and 5 min. dwell time. (Sample # Z22)

Figure IV-19. a & b Micrographs of microwave sintered zirconia at 4 different dwell times and at 1460°C.*

* All micrographs are digitally filtered with PhotoShop High-Pass filter.

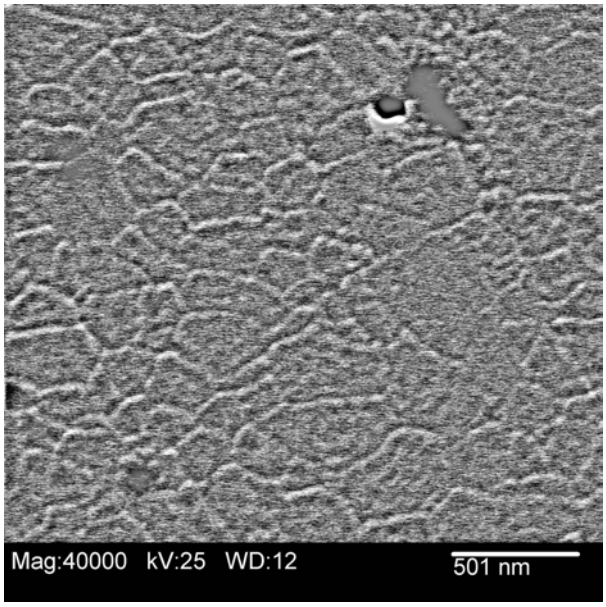

(c) Microwave sintered zirconia at 1460°C and 10 min. dwell time. (Sample # Z32)

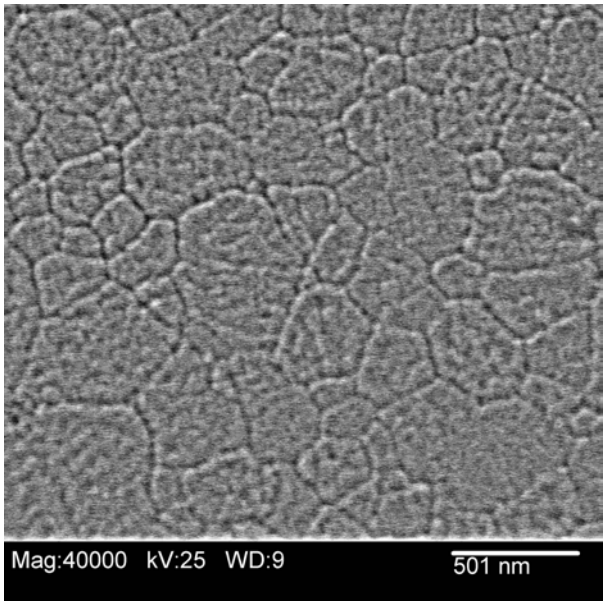

(d) Microwave sintered zirconia at 1460°C and 15 min. dwell time. (Sample # Z42)

Figure IV-19. c & d Micrographs of microwave sintered zirconia at 4 different dwell times and at 1460°C.*

* All micrographs are digitally filtered with PhotoShop High-Pass filter.

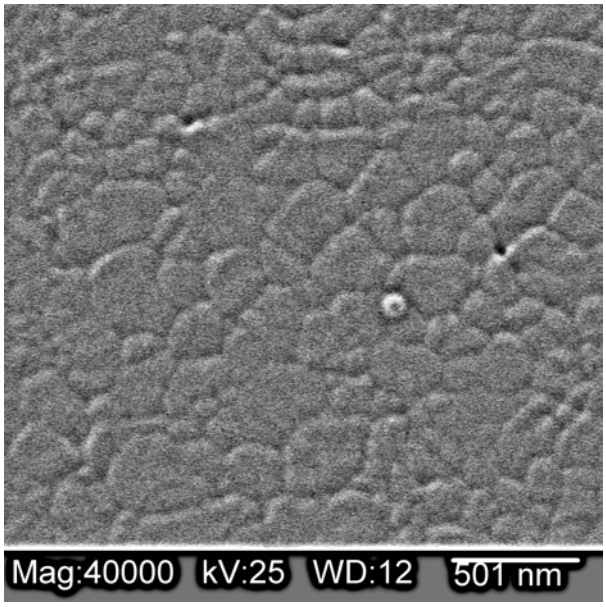

(a) Microwave sintered zirconia at 1480°C and 0 min. dwell time. (Sample # Z13)

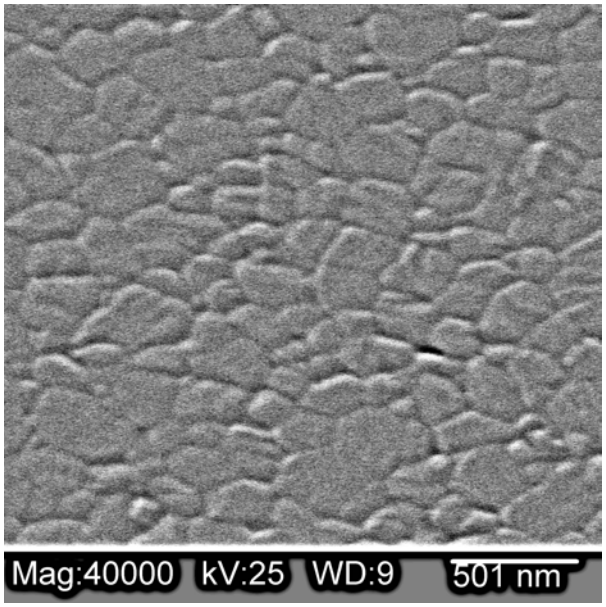

(b) Microwave sintered zirconia at 1480°C and 5 min. dwell time. (Sample # Z23)

Figure IV-20. a & b Micrographs of microwave sintered zirconia at 4 different dwell times and at 1480°C.*

* All micrographs are digitally filtered with PhotoShop High-Pass filter.

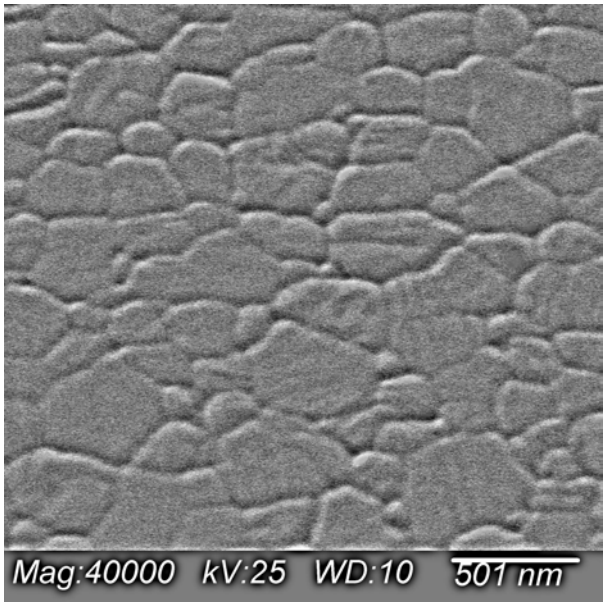

(c) Microwave sintered zirconia at 1480°C and 10 min. dwell time. (Sample # Z33)

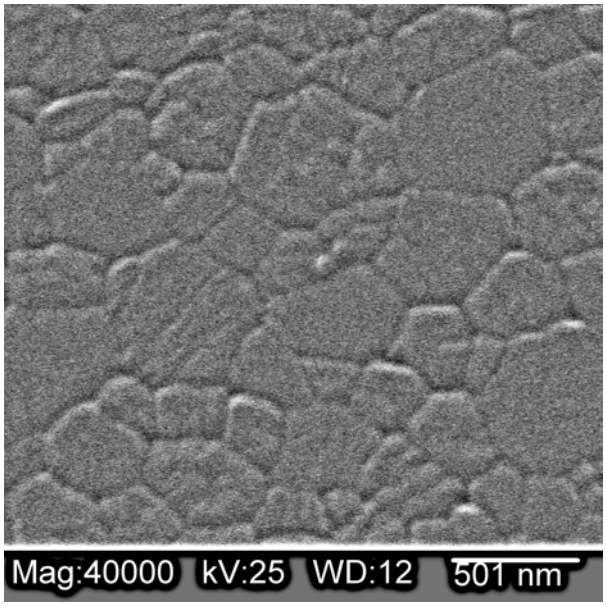

(d) Microwave sintered zirconia at 1480°C and 15 min. dwell time. (Sample # Z43)

Figure IV-20. c & d Micrographs of microwave sintered zirconia at 4 different dwell times and at 1480°C.*

* All micrographs are digitally filtered with PhotoShop High-Pass filter.

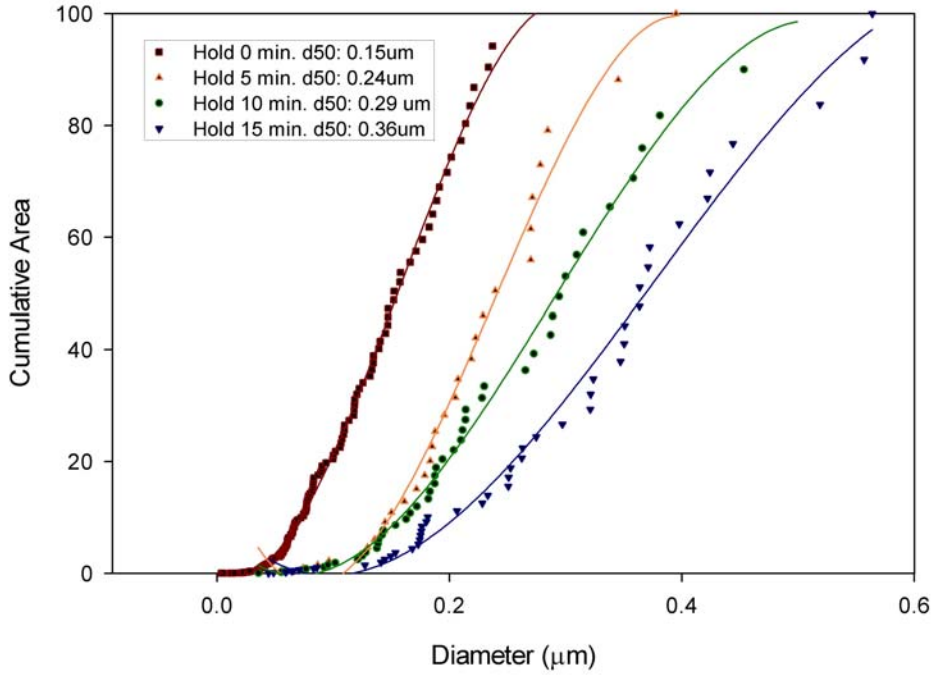

Figure IV-21. Grain size distribution of microwave sintered zirconia samples with different dwell times at 1460°C.

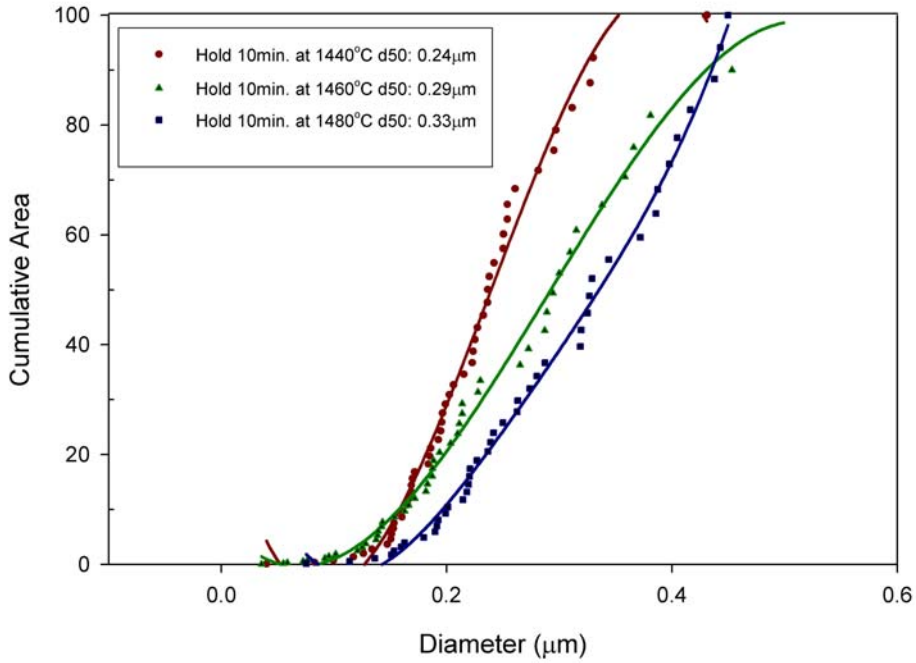

Figure IV-22. Grain size distribution of microwave sintered zirconia samples at different temperatures with 10 min. dwell time.

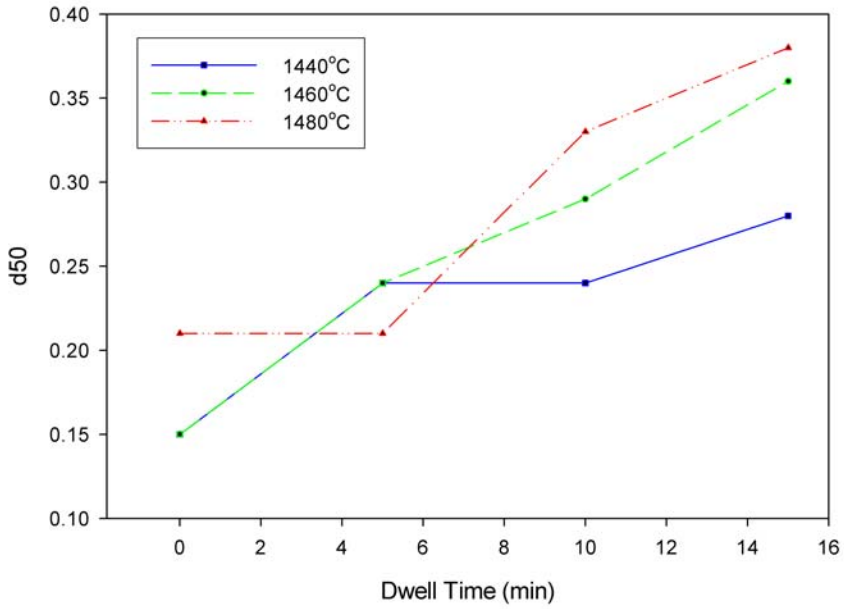

Figure IV-23. Average grain sizes of the microwave sintered zirconia samples at different temperatures and dwell times.

Polycrystalline materials sinter by diffusional transportation of material. And the paths of material transportation define the mechanism of transportation. Basic transportation paths are: surface diffusion, lattice diffusion, vapor transport and grain boundary diffusion.

Densification and grain growth occurs as a result of diffusion and diffusion is a time-dependent phenomena. With longer dwell times grain sizes increases, Equation 12 shows time dependence of the grain size. Where D is the grain size at time t, D_o is the grain size at t_o and K is a rate constant.

$$D = D_o + Kt^{1/2} \qquad (12)$$

Figures IV-18 through IV-20 show the micrographs of the zirconia samples. Fig. IV-21 and Fig. IV-23 show the effect of dwell time on grain size of zirconia samples. As the dwell time increases grain size increases due to high amount of material diffusion. High temperature also helps diffusion and increases its speed by introducing more energy into the system. As can be seen on Fig. IV-22 size of the zirconia grains increased by increased temperature.

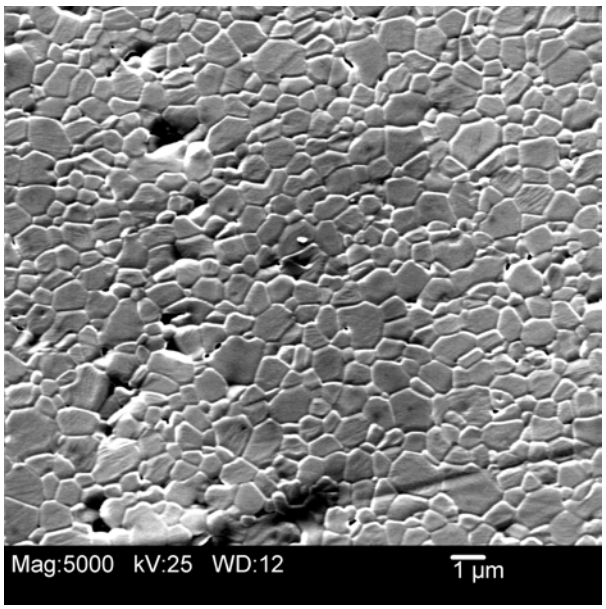

(a) Microwave sintered alumina at 1480°C and 15 min. dwell time. (Sample # A21)

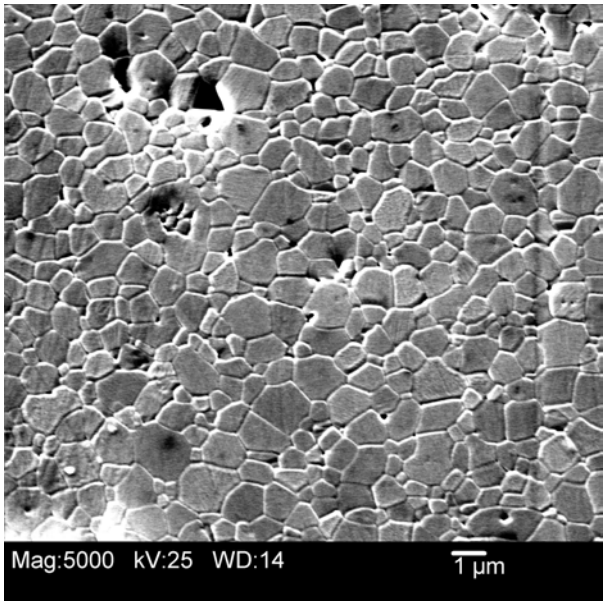

(b) Microwave sintered alumina at 1500°C and 15 min. dwell time. (Sample # A22)

Figure IV-24. a & b Micrographs of microwave sintered alumina at different temperatures and dwell times.

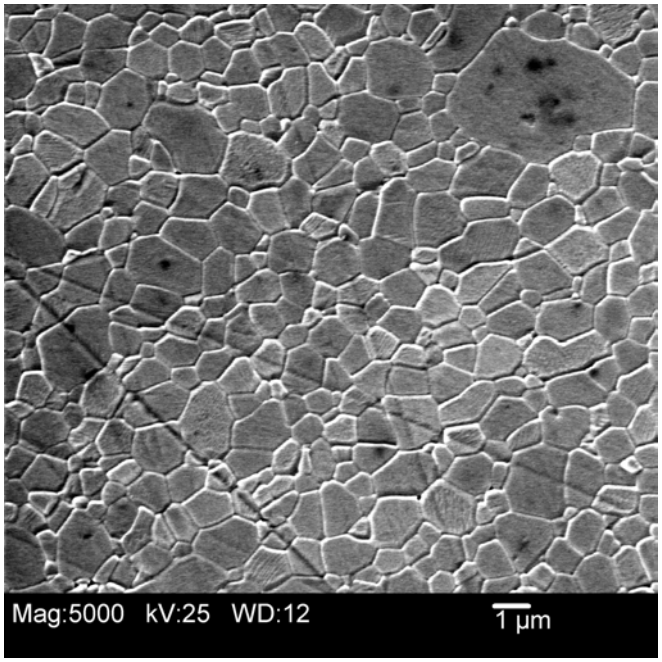

(c) Microwave sintered alumina at 1520°C and 15 min. dwell time. (Sample # A23)

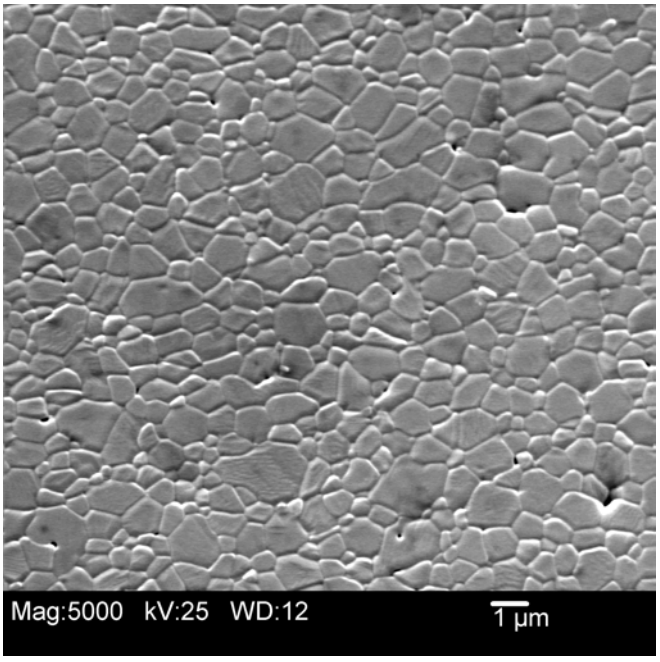

(d) Microwave sintered alumina at 1500°C and 10 min. dwell time. (Sample # A12)

Figure IV-24. c & d Micrographs of microwave sintered alumina at different temperatures and dwell times.

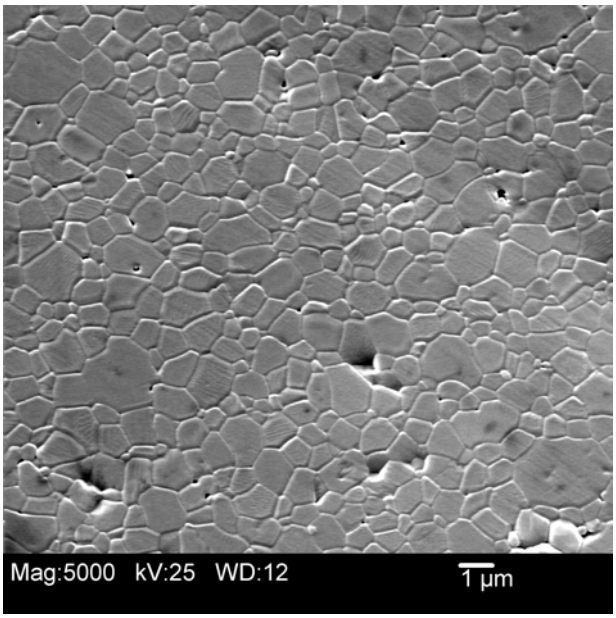

(e) Microwave sintered alumina at 1520°C and 20 min. dwell time. (Sample # 32)

Figure IV-24. (e) Micrographs of microwave sintered alumina at different temperatures and dwell times.

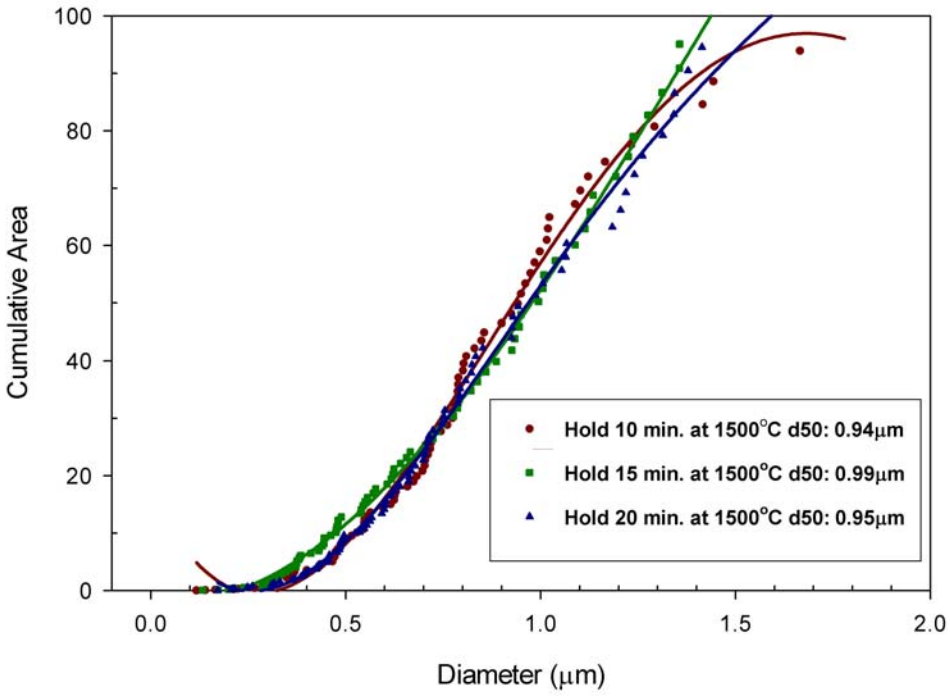

Figure IV-25. Grain size distribution of microwave sintered alumina samples with different dwell times at 1500°C.

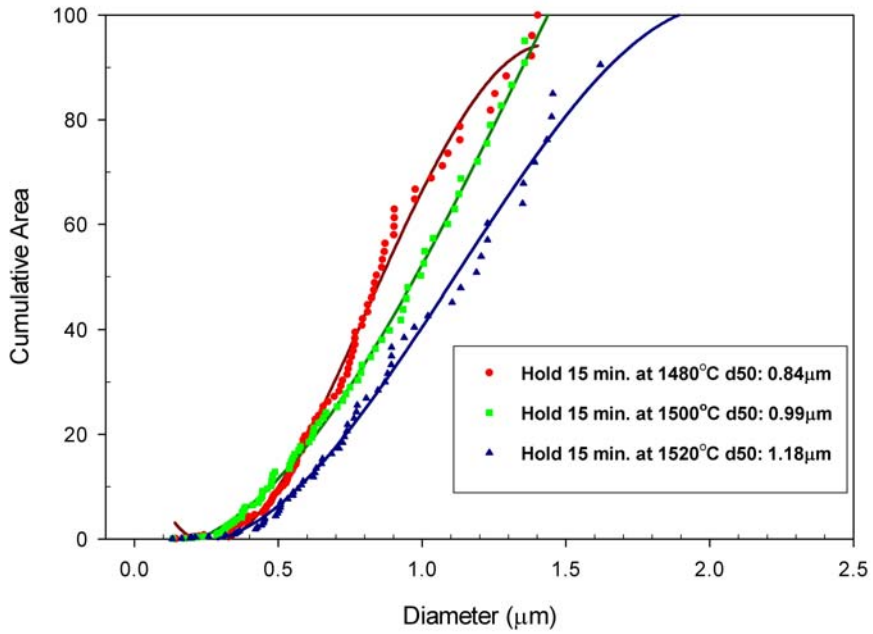

Figure IV-26. Grain size distribution of microwave sintered alumina samples at different temperatures with 15 min. dwell time.

Figure IV-24 shows the micrographs of the alumina samples sintered at different time and temperatures. Fig. IV-25 and Fig. IV-26 show the effect of time and temperature on grain size of the alumina samples. Increasing of dwell time did not affect the grain size of alumina samples too much when compared with Fig. IV-21 of zirconia samples. The main driving force for grain growth is the decrease in grain boundary energy which results from a decrease in the grain boundary area. The driving force for grain growth is inversely proportional to the size of grains, a sample with smaller grain size (large grain boundary area) will have more driving force when compared to a sample with large grains (small grain boundary area). Because of this effect of grain size on driving force of grain growth, alumina samples did not show a big difference in their grain sizes when sintered at different dwell times. The particle size for alumina powder was 0.35 μm and 0.035 μm for zirconia powder. But increasing the temperature made an effect on grain size of the alumina samples too (Fig. IV-26), because increased temperature made the diffusion faster by introducing energy to the system.

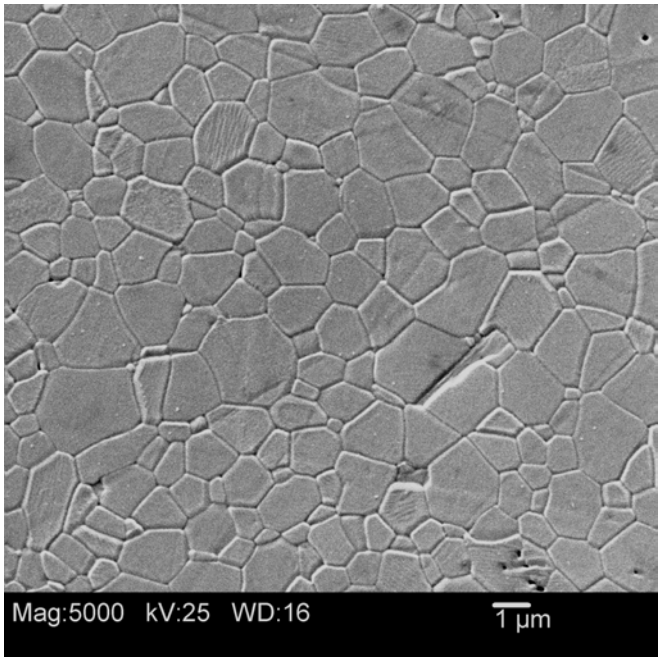

(a) Conventionally sintered alumina at 1540°C and 1 hour dwell time. (Sample # AC1)

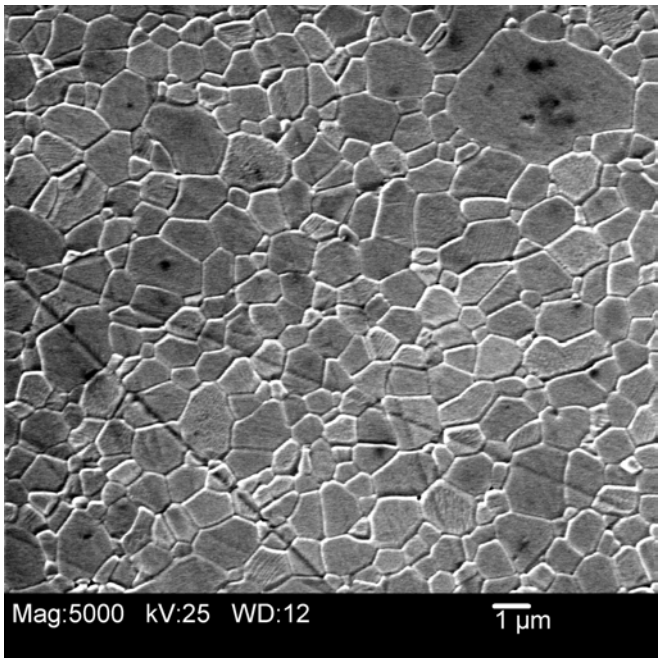

(b) Microwave sintered alumina at 1520°C and 15 min dwell time. (Sample # A23)

Figure IV-27. Micrographs of conventionally (a) and microwave (b) sintered alumina samples.

Fig. IV-27 a & b shows the microstructure difference between conventionally and microwave sintered alumina samples. The d50 for conventionally sintered alumina was 1.40 μm and for microwave sintered alumina was 1.18 μm. Their theoretical densities were almost same 99. 8% TD for conventional sintered sample and 99.4% TD for microwave sintered one. According to S. A. Nightingale[28] microwaves tend to accelerate lattice diffusion more than surface and grain-boundary diffusion. This specific increase in lattice diffusion increases densification while keeping the grain growth rate low. As a result of this effect high densifications can be achieved when the grain sizes are small.

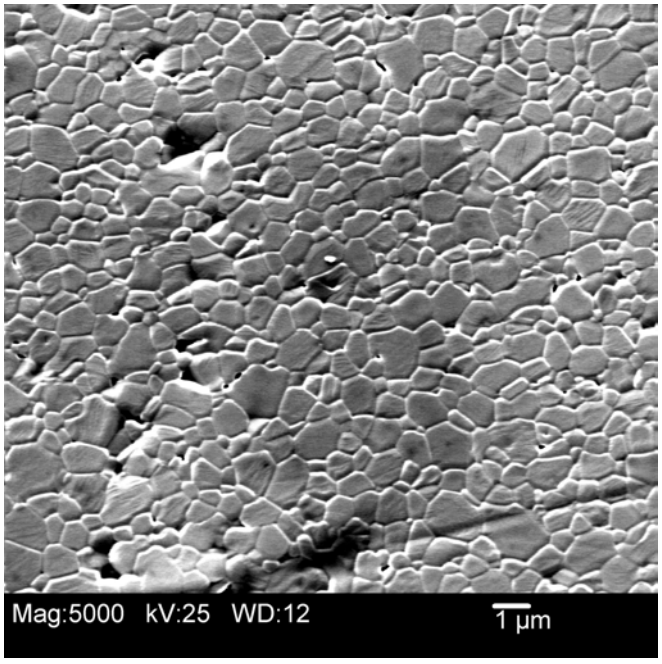

(a) Microwave sintered alumina at 1480°C with 15 min. dwell time. (Sample # A21)

Figure IV-28. (a) Micrograph of microwave sintered alumina sample.

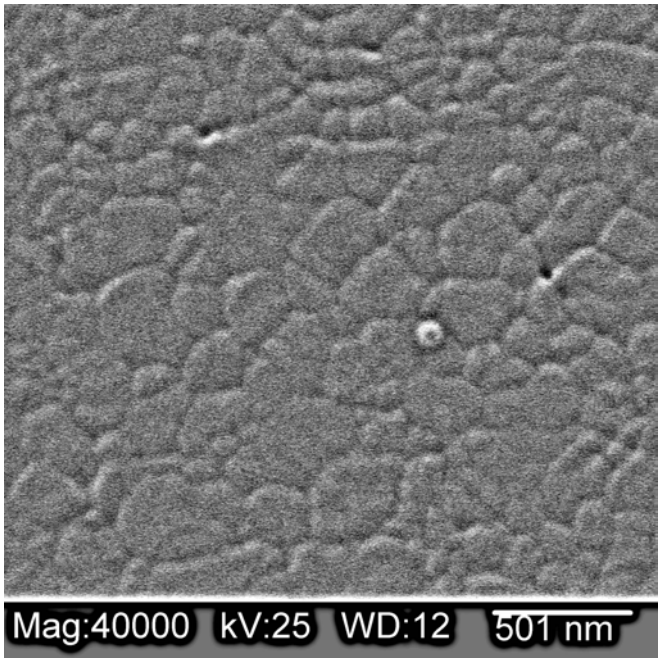

(b) Microwave sintered zirconia at 1480°C with 15 min. dwell time. (Sample # Z43)

Figure IV-28. (b) Micrograph of microwave sintered zirconia sample.

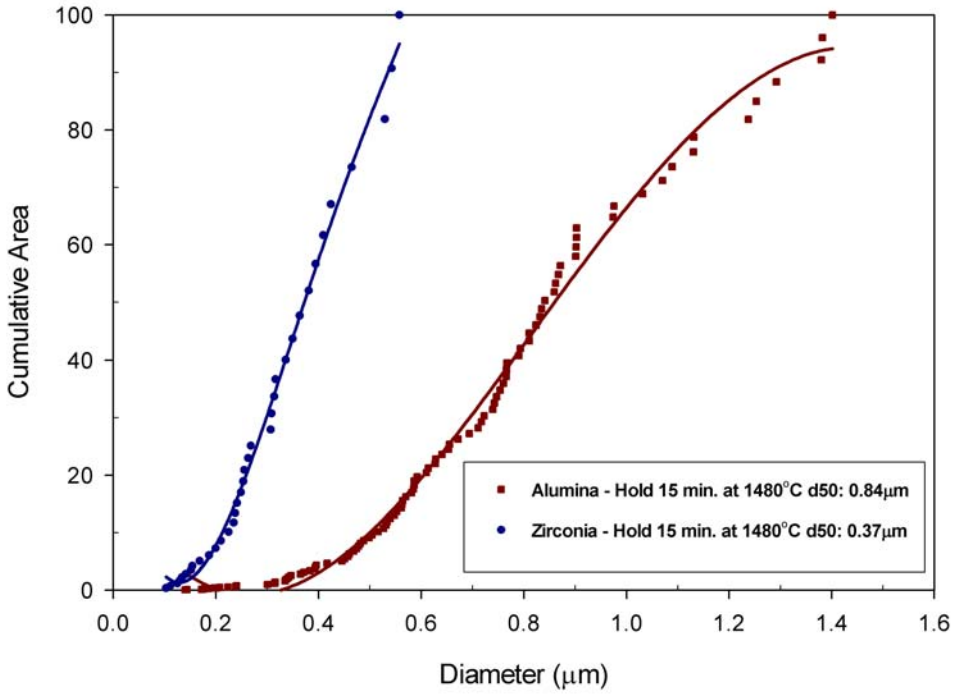

Figure IV-29. Grain size distribution of microwave sintered alumina and zirconia.

Figure IV-28 shows the microstructural differences between the microwave sintered alumina (a) and zirconia (b) samples. They were both sintered at the same temperature and same dwell time, 1480°C and 15 min. Zirconia has much smaller grains compared to alumina (check the scale). As can be seen on Fig. IV-29, d50 value for zirconia is 0.37 μm and for alumina it is 0.84 μm. Their densities were 99.2% TD and 97.9% TD for alumina and zirconia, respectively. The density difference can be attributed to the particle size differences (0.35 μm alumina powder, 0.035 μm zirconia powder). Smaller particles have higher surface area which increases the number of necks between particles in the sintering process and this leads to a higher densification at a lower temperature compared to densifications of low surface area particles, as in the case for alumina. The other reason for high densification is the high driving force for diffusion in high surface area powders. As mentioned before, sintering is a diffusion controlled process and if the driving force is high, sintering occurs faster and at low temperatures.

6. Effect of Number of "Boxes" on Temperature

In all of the above experiments only one box was used and only one sample sintered at a time, because microwave sintering depends on the amount of material used. Fig. IV-30 shows maximum temperature reached when two insulation boxes (including 2 additional susceptor and an additional sample) were used instead of one box set.

One of the boxes located on spot #2 to get the accurate temperature and the other box located on spot #3 since it was the most efficient spot from Fig. IV-5. Table III-II was used as the power profile. The same set-up repeated with only one box at spot #2 for the second run.

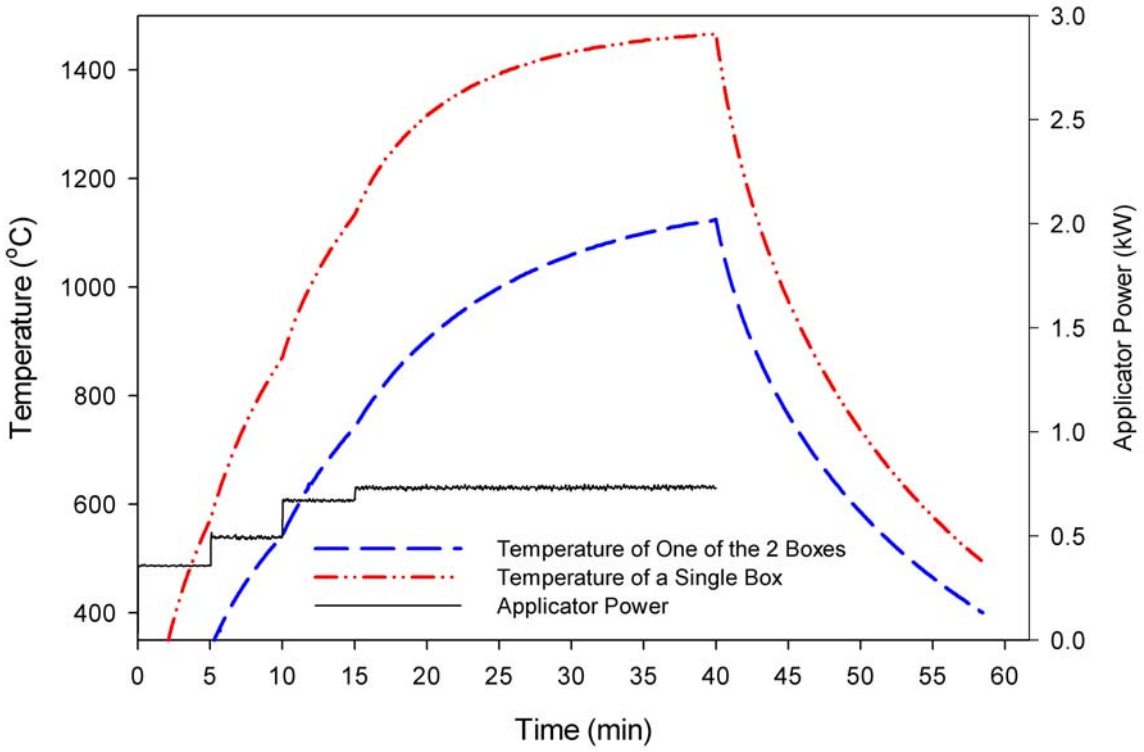

Figure IV-30. Temperature reading for single and 2 boxes at a time.

Materials absorb the microwaves and heat up. In the present case SiC susceptors are high microwave absorbers. They are used as the "coupling" material absorbing the microwave energy even at low (room temp.) temperatures. The absorbed energy is then transferred through radiative heat exchange to the mostly microwave transparent samples. When the amount of absorbing material is increased then the amount of microwave energy per g-sample will effectively decrease. This explains the lower temperature when two boxes were used instead of one (Fig. IV-30).

7. Energy Consumption Comparison (MW vs Conventional heating)

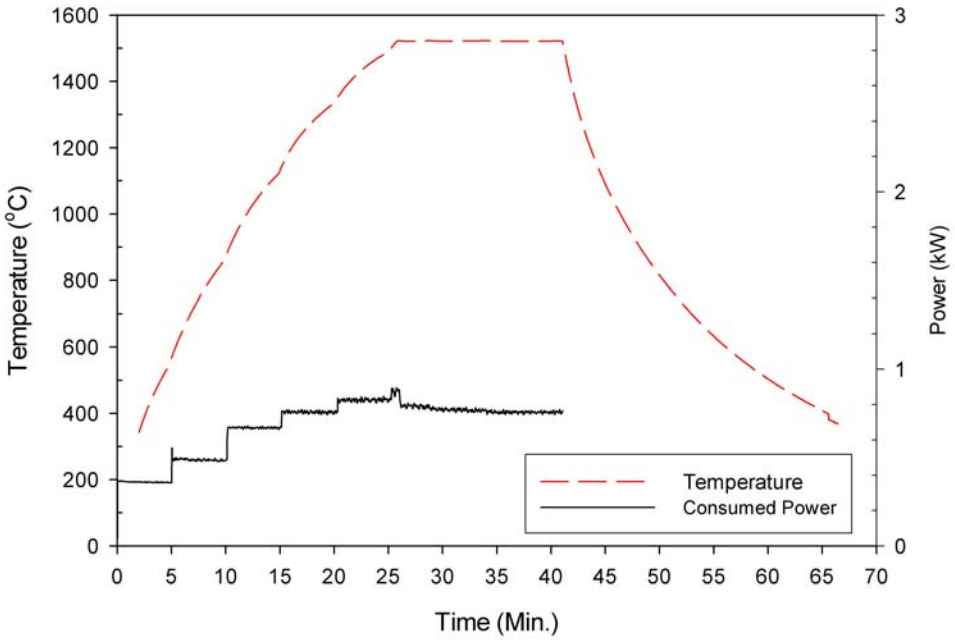

Figure IV-31. Temperature and energy graph for MW sintering of alumina.

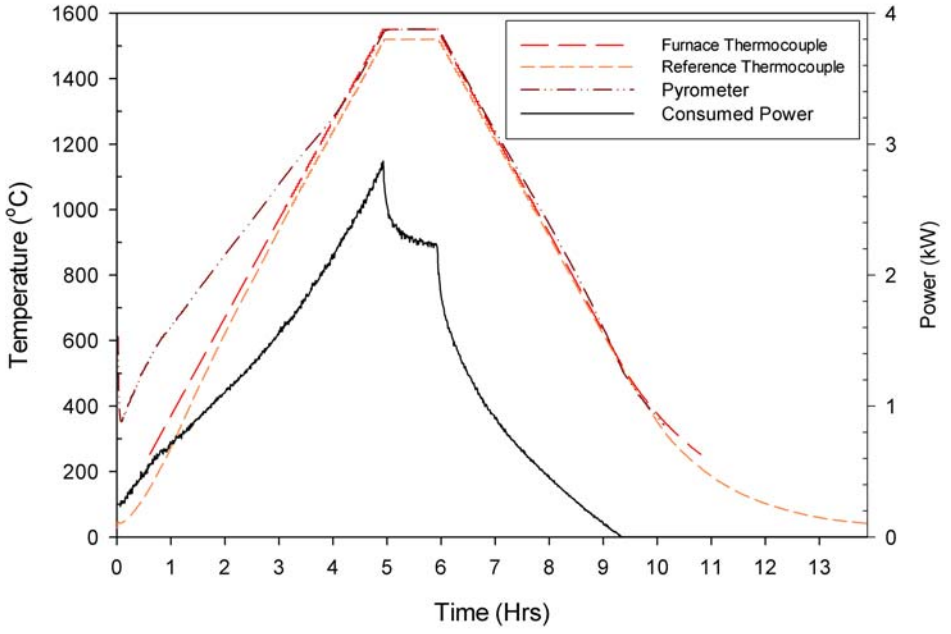

Figure IV-32. Temperature and energy graph for conventional sintering of alumina.

Fig. IV-31 and Fig. IV-32 show the temperature and used energy graphs for MW and conventional sintering of an alumina sample, respectively. In microwave sintering, the temperature was increased up to 1520°C and was kept at that temperature for 15 min. For the case of conventional sintering, temperature was increased up to 1550°C and kept at that temperature for 1hr. At the end of both sintering processes samples of almost the same densities were achieved. 99.5 % and 99.8 % theoretical density for MW and conventional sintering, respectively. But the energy and time consumed for those experiments was different. The energy consumed during the MW sintering was only 0.46 kW h while it was 11.54 kW h for the conventional sintering. (Consumed power calculated from the area under the power curve in Figures IV-31 and IV-32.) In addition the total sintering time cycle was around 1h for microwave sintering and 10 h. for conventional sintering.

C. Microwave and Conventional Sintering of RP Printed Samples

Alumina slurries prepared according to compositions that are given in Table III-IV. After 20 h. ball milling, preprepared 2wt% alginate solution added with the amounts described in Table III-IV. Those slurries used to print 1" diameter disks with the SGP method. Printed disks sintered with conventional and microwave methods at 1500°C for 15min.

Table IV-V shows the resulting theoretical densities of the samples.

Table IV-V Theoretical Densities of the Printed Samples of Different Slurries

	Darvan Concentration	Slurry Viscosity (cps)*	Conventional Sintering TD	Microwave Sintering TD
B1	0.85 wt%	588	86.9 %	87.6 %
B2	0.60 wt%	648	82.9 %	81.2 %
B3	1.20 wt%	628	93.9 %	93.1 %

* Viscosity measure with Brookfield Digital viscometer at 100 rpm.

There was a significant increase in sintered density of slurry B3. Slurry B3 had the highest amount of Darvan (1.20 wt%). This could be the reason for the high density values of those samples. Higher amounts of Darvan give high dispersions but since 1.20wt% is slightly out of range for the low viscosity, this slurry might have a slightly higher viscosity. Higher viscosities decrease the accuracy of printing. As a matter of fact, slurry B1 was the only slurry which gave a decent print quality. None of the other slurries gave an acceptable print quality.

The highest achieved density of microwave sintered SGP printed sample was ~93% TD. However, at the same time-temperature profile (1500°C and 15 min. dwell time) the density of microwave sintered pressed sample was ~98% TD. This difference mostly caused from the low packing density of the SGP printed samples. Pressed samples had high green density because of their high packing, and this high green density resulted a higher sintered density when compared to SGP printed samples.

V CONCLUSION

The present study demonstrated the way to produce a ceramic part in a very fast way starting from a design and ending as a dense sintered product. Selective Gelation Printing was used as the green product production method. Its ability to build very complex shapes in a relatively short period of time makes it very useful for unique product productions like knee and hip implants.

The Selective Gelation Printing is still under further development, some of the problems encountered in printing experiments were: Drying of the top layer of slurry on build table, sticking of printed layers to doctor-blade and shape deterioration while washing (edges round off).

When a high solid content was used, the drying of the slurry became a severe problem. Since the top layer of slurry on build table is directly exposed to air slurry was drying very fast which then made the printing process impossible. This problem could be solved by increasing the humidity of the environment or by decreasing the solid content in the slurry. Since, high solid content was one of the goals of the study to achieve high sintered densities, the latter solution is not recommended.

While removing the ungeled portion (slurry) of the printed samples during the washing process, some of the gelled material along the edges was also dissolved in the water. Freeze-drying could be a solution to this problem. In addition a CaCl bath could be used after the water-washing to increase the strength of the gelled product.

Microwave sintering was chosen to make the whole process even faster. Similar to the SGP process, microwave sintering is also a new method and still under further development. In this study SiC susceptors were used to initially heat-up the sample until the sample could directly couple with the microwaves. The advantage of microwave sintering is its speed and low energy consumption. Microwave sintering was approximately 20 times efficient than the conventional sintering, with respect to energy consumption and microwave heating was ~10 times faster when compared with conventional sintering. However, those numbers are based on one single sample sintered at a time. Conventional sintering becomes more efficient when more than one sample is sintered since the required energy increases only by a relative small percentage.

However in microwave processing every additional sample requires a much larger relative increase in the required input energy (power). Since, this was a study on rapid prototyping of custom designed single products, most of the time only one sample will need to be prepared and sintered at a time. Under these conditions microwave sintering saves a lot of time and energy when compared to conventional heating.

The combination of selective gelation printing and microwave sintering has a lot of potential for the fast production of individual ("one of a kind") or short run productions (<25) of ceramic knee and hip implants.

VI FUTURE WORK

Effect of slurry composition, layer thickness and calcium concentration on printing resolution and surface roughness of the printed samples can be further studied. Solid content of the slurries can be studied by using different dispersants like Duramax instead of Darvan or additional chemicals like glycerol.

Aging effects of SiC susceptors and insulation box can be studied. Effect of different SiC susceptors (supplier, size and shape) can also be further studied and compared with the results of this study. A diffusion couple can be used to study the effect of microwaves on diffusion mechanisms.

REFERENCES

1. C. Griffin, J. Daufenbach, and S. McMillin, "Desktop Manufacturing LOM vs Pressing," *Am. Ceram. Soc. Bull.,* **75** [5] 109-13 (1994).

2. M. L. Griffith, T. M. Chu, W. C. Wagner, and J. W. Halloran, "Ceramic Stereolithography for Investment Casting and Biomedical Applications," *Solid Freeform Fabr. Symp. Proc.,* **6,** 31-8 (1995).

3. M. K. Agarwala, R. V. Weeren, R. Vaidyanathan, and A. Bandhopadhyay, "Structural Ceramics by Fused Deposition Ceramics," *Solid Freeform Fabr. Symp. Proc.,* **6,** 1-8 (1995).

4. D. L. Bourell, H. L. Marcus, J. W. Barlow, and J. J. Beaman, "Selective Laser Sintering of Metals and Ceramics," *Int. J. Powder Metall. (N. Y.),* **28** [4] 369-81 (1992).

5. U. Laksminaray, S. Ogrydiziak, and H. L. Marcus, "Selective Laser Sintering of Ceramic Materials," *Solid Freeform Fabr. Symp. Proc.,* **1,** 16-26 (1990).

6. E. Sachs, M. Cima, P. Williams, D. Brancazio, and J. Cornie, "Three Dimensional Printing: Rapid Tooling and Prototypes Directly from a CAD Model," *J. Eng. Ind.,* **114** [4] 481-8 (1990).

7. E. Sachs, M. Cima, and J. Cornie, "Three Dimensional Printing: Rapid Tooling and Prototypes Directly from CAD Representation," *Solid Freeform Fabr. Symp. Proc.,* **1,** 27-47 (1990).

8. M. J. Cima and E. M. Sachs, "Three Dimensional Printing: Form, Materials and Performance," *Solid Freeform Fabr. Symp. Proc.,* **2,** 187-94 (1991).

9. J. D. Cawley, A. H. Heuer, W. S. Newman, and B. B. Mathewson, "Computer-aided Manufacturing of Laminated Engineering Materials," *Am. Ceram. Soc. Bull.,* **75** [5] 75-9 (1996).

10. S. Baskaran, G. D. Maupin, and G. L. Graff, "Freeform Fabrication of Ceramics," *Am. Ceram. Soc. Bull.,* **77** [7] 53-8 (1998).

11. K. Clare, "Algin," Ch. 6 in *Industrial Gums - Polysaccharides and Their Derivatives.* Edited by J. N. B. Roy L. Whistler. Academic Press, London, 1993.

12. R. J. Glennon and T. L. V. Winkle, "The Multifunctional Role of Alginates and Xanthan Gum In processing Alumina and Other Ceramic Bodies," *Proc, Annu. Meet. Jt. Fall Meet. – Am. Ceram. Soc., Mater. Equip. Whitewares Div.,* **2**, 81-3 (1976).

13. J. Lyklema, Ch. 3 in *Colloidal Dispersions.* Edited by J. W. Goodwin. The Royal Society of Chemistry, London, 1982.

14. S. W. Sofie and F. Dogan, "Freeze Casting of Aqueous Alumina Slurries with Glycerol," *J. Am. Ceram. Soc.,* **84** [7] 1459-64 (2001).

15. M. N. Rahaman, "Science of Colloidal Processing," Ch. 15 in *Ceramic Processing and Sintering.* Marcel Dekker, New York, 1995.

16. R. F. Conley, "Organic Polyacid Salt Dispersions," Ch. 4 in *Practical Dispersion - A Guide to Understanding and Formulating Slurries.* VCH, Albuquerque, NM, 1996.

17. V. A. Hackley, "Development of Electroacoustic Methods and Their Application in Ceramic Processing," pp. 237-59 in *Advances in Process Measurements for the Ceramic Industry.* Edited by A. Jillavenkatesa and G. Y. Onoda. The American Ceramic Society, Westerville, Ohio, 1999.

18. R. W. O'Brien, D. W. Cannon, and W. N. Rowlands, "Electroacoustic Determination of Particle Size and Zeta Potential," *J. Colloid Interface Sci.,* **173** [2] 406- 18 (1995).

19. C. Zhao, J. Vleugels, C. Groffils, P. J. Luypaert, and O. V. D. Biest, "Hybrid Sintering with a Tubular Susceptor in a Cylindrical Single-mode Microwave Furnace," *Acta Materialia,* **48** [14] 3795-801 (2000).

20. D. E. Clark and D. C. Folz, "Developments in Microwave Processing Technologies," *Ceram. Eng. Sci. Proc.,* **18** [4] 531-41 (1997).

21. L. M. Sheppard, "Manufacturing Ceramics with Microwaves: The Potential for Economical Production," *Am. Ceram. Soc. Bull.,* **67** [10] 1656-61 (1988).

22. K. Y. Lee and E. D. Case, "Microwave Joining and Repair of Ceramics and Ceramic Composites," *Ceram. Eng. Sci. Proc.,* **18** [4] 543-50 (1997).

23. W. H. Sutton, "Microwave Processing of Ceramic Materials," *Am. Ceram. Soc. Bull.,* **68** [2] 376-86 (1989).

24. T. T. Meek, R. D. Blake, and J. J. Petrovic, "Microwave Sintering of Al_2O_3 and Al_2O_3-SiC Whisker Composites," *Ceram. Eng. Sci. Proc.,* **8** [7-8] 861-71 (1987).

25. W. W. Ho, "High-Temperature Dielectric Properties of Polycrystalline Ceramics," pp. 137- 48, *Microwave Processing of Materials.* Edited by W. H. Sutton, M. H. Brooks, I. J. Chabinsky. Materials Research Society, Pittsburgh, PA, 1988.

26. M. A. Janney, C. L. Calhoun, and H. D. Kimrey, "Microwave Sintering of Solid Oxide Fuel Cell Materials: I, Zirconia-8 mol% Yttria," *J. Am. Ceram. Soc.,* **75** [2] 341-6 (1992).

27. R. Z. Chen and W. H. Tuan, "Thermal Etching of Alumina," *Am. Ceram. Soc. Bull.,* **79** [10] 83-6 (2000).

28. S. A. Nightingale, D. P. Dunne, and H. K. Worner, "Sintering and Grain Growth of 3 mol % Yttria Zirconia in a Microwave Field," *J. Mater. Sci.,* **31** [19] 5039-43 (1996).

Table of Samples Used in Microwave Experiments

Sample #	Material	Preparation Method		Sintering Method			Time- Temp. - Power			Hardness (VHN)	Theoretical Density %	Grain Size	Microstr. Pg.
		Pressing	SGP	Microwave	Pos #	Conv.	Power	Dwell Time	Temp.				
Z11	Zirconia	X		X	2			0 min.	1440°C	608 ±12	82.2 (81.8)	0.15 μm	48
Z21	Zirconia	X		X	2			5 min.	1440°C	1063 ±13	95.0 (94.4)	0.24 μm	48
Z31	Zirconia	X		X	2			10 min.	1440°C	1123 ±23	96.3 (96.4)	0.24 μm	49
Z41	Zirconia	X		X	2			15 min.	1440°C	1142 ±13	95.9 (95.6)	0.28 μm	49
Z12	Zirconia	X		X	2			0 min.	1460°C	738 ±81	85.4 (85.7)	0.15μm	50
Z22	Zirconia	X		X	2			5 min.	1460°C	1207 ±31	95.7 (96.0)	0.24 μm	50
Z32	Zirconia	X		X	2			10 min.	1460°C	1278 ±39	96.7 (96.1)	0.29 μm	51
Z42	Zirconia	X		X	2			15 min.	1460°C	1284 ±18	96.6 (96.2)	0.36 μm	51
Z13	Zirconia	X		X	2			0 min.	1480°C	888 ±12	91.3 (91.2)	0.21 μm	52
Z23	Zirconia	X		X	2			5 min.	1480°C	1213 ±25	97.0 (98.6)	0.21 μm	52
Z33	Zirconia	X		X	2			10 min.	1480°C	1223 ±23	98.6 (99.0)	0.33 μm	53
Z43	Zirconia	X		X	2			15 min.	1480°C	1264 ±16	99.2 (98.0)	0.38 μm	53
A12	Alumina	X		X	2			10 min.	1500°C	1650 ±62	97.7 (96.8)	0.94 μm	57
A22	Alumina	X		X	2			15 min.	1500°C	1690 ±31	98.3 (98.8)	0.99 μm	56
A32	Alumina	X		X	2			20 min.	1500°C	1718 ±44	99.0 (98.0)	0.95 μm	58
A21	Alumina	X		X	2			15 min.	1480°C	1613 ±46	97.9 (96.7)	0.84 μm	56
A23	Alumina	X		X	2			15 min.	1520°C	1701 ±40	99.4 (99.7)	1.18 μm	57

Sample #	Material	Preparation Method		Sintering Method			Time- Temp. - Power			Hardness (VHN)	Theoretical Density %	Grain Size	Microstr. Pg.
		Pressing	SGP	Microwave	Pos #	Conv.	Power	Dwell Time	Temp.				
ZM1	Zirconia	X		X	1		Table III-II	0 min.	N/A		96.3		
ZM2A	Zirconia	X		X	2		Table III-II	0 min.	1470°C		97.8		
ZM2B	Zirconia	X		X	2		Table III-II	0 min.	1470°C		98.8		
ZM3A	Zirconia	X		X	3		Table III-II	0 min.	N/A		98.9		
ZM3B	Zirconia	X		X	3		Table III-II	0 min.	N/A		98.0		
ZM4	Zirconia	X		X	4		Table III-II	0 min.	N/A		93.9		
ZM5A	Zirconia	X		X	5		Table III-II	0 min.	N/A		95.2		
ZM5B	Zirconia	X		X	5		Table III-II	0 min.	N/A		94.5		
ZM6	Zirconia	X		X	6		Table III-II	0 min.	N/A		94.4		
ZM7A	Zirconia	X		X	7		Table III-II	0 min.	N/A		92.0		
ZM7B	Zirconia	X		X	7		Table III-II	0 min.	N/A		90.9		
ZM8	Zirconia	X		X	8		Table III-II	0 min.	N/A		95.8		
ZM9	Zirconia	X		X	9		Table III-II	0 min.	N/A		95.7		
AC1	Alumina	X				X		1 hr.	1540		97.8	1.40 μm	60
B1M	Alumina		X	X	2			15 min.	1500°C		87.6		
B2M	Alumina		X	X	2			15 min.	1500°C		81.2		
B3M	Alumina		X	X	2			15 min.	1500°C		93.1		

Sample #	Material	Preparation Method		Sintering Method			Time- Temp. - Power			Hardness (VHN)	Theoretical Density %	Grain Size	Microstr. Pg.
		Pressing	SGP	Microwave	Pos #	Conv.	Power	Dwell Time	Temp.				
BC1	Alumina		X			X		15 min.	1500°C		86.9		
BC2	Alumina		X			X		15 min.	1500°C		82.9		
BC3	Alumina		X			X		15 min.	1500°C		93.9		